The induction of reentry in cardiac tissue. The missing link: How electric fields alter transmembrane potential

Article *in* Chaos (Woodbury, N.Y.) · April 1998

DOI: 10.1063/1.166298 · Source: PubMed

2 authors, including:

Bradley J Roth
Oakland University
307 PUBLICATIONS **7,744** CITATIONS

SEE PROFILE

The induction of reentry in cardiac tissue. The missing link: How electric fields alter transmembrane potential

Bradley J. Roth[a)]
Department of Physics and Astronomy, Vanderbilt University, Nashville, Tennessee 37235

Wanda Krassowska
Department of Biomedical Engineering and Duke-North Carolina NSF/ERC, Duke University, Durham, North Carolina 27708-0281

(Received 2 June 1997; accepted for publication 21 September 1997)

This review examines the initiation of reentry in cardiac muscle by strong electric shocks. Specifically, it concentrates on the mechanisms by which electric shocks change the transmembrane potential of the cardiac membrane and create the physiological substrate required by the critical point theory for the initiation of rotors. The mechanisms examined include (1) direct polarization of the tissue by the stimulating current, as described by the one-dimensional cable model and its two- and three-dimensional extensions, (2) the presence of virtual anodes and cathodes, as described by the bidomain model with unequal anisotropy ratios of the intra- and extracellular spaces, (3) polarization of the tissue due to changing orientation of cardiac fibers, and (4) polarization of individual cells or groups of cells by the electric field (''sawtooth potential''). The importance of these mechanisms in the initiation of reentry is examined in two case studies: the induction of rotors using successive stimulation with a unipolar electrode, and the induction of rotors using cross-field stimulation. These cases reveal that the mechanism by which a unipolar stimulation induces arrhythmias can be explained in the framework of the bidomain model with unequal anisotropy ratios. In contrast, none of the examined mechanisms provide an adequate explanation for the induction of rotors by cross-field stimulation. Hence, this study emphasizes the need for further experimental and theoretical work directed toward explaining the mechanism of field stimulation.
 [S1054-1500(98)00601-6]

Electrical stimulation of the heart consists of the following chain of events: 1) the placement of stimulating electrodes and the geometry and structure of the tissue determine the electric field that is established in the heart; 2) this electric field alters the transmembrane potential, i.e., the potential existing across the membranes of cardiac cells; 3) this transmembrane potential changes the physiological state of the membrane, resulting in excitation, induction of reentry, or defibrillation. The electric field in the heart is determined by an elliptic partial differential equation with appropriate boundary conditions. Moreover, given the distribution of the transmembrane potential, the induction of reentry is explained by critical point theory. In contrast, the connection between the electric field and the transmembrane potential is the ''missing link'' in our knowledge of electrical stimulation. This connection is not explained adequately by a basic mathematical model of the electrical activity of the heart: a single reaction-diffusion equation. In that model, the transmembrane potential has a physiologically significant magnitude only within a few length constants of the electrode. To determine how the shock affects the tissue away from the electrode, the model must incorporate other mechanisms, such as virtual electrodes, the changing orientation of cardiac fibers, and cellular and macroscopic discontinuities. This paper concentrates on the mechanisms by which an electric field alters the transmembrane potential, and their role in the induction of reentry.

I. INTRODUCTION

The dashed oval in Fig. 1 encloses the topics covered in this review. Section II reviews the critical point theory. Section III demonstrates how experimental evidence forces one to confront the missing link in order to use the critical point theory to understand the induction of rotors in cardiac tissue. Section IV reviews the known mechanisms by which an electric field induces a transmembrane potential, V_m. The importance of these mechanisms is illustrated by a detailed analysis of two case studies: the induction of reentry by successive stimulation through a single, unipolar electrode (Sec. V), and the induction of reentry by cross-field stimulation (Sec. VI). A careful examination of experimental studies of reentry induction supports or refutes different hypotheses about how an electric field alters V_m, and suggests that additional modeling and experimental studies are needed to completely understand the missing link (Sec. VII).

II. CRITICAL POINT THEORY

The most widely accepted theory for the induction of reentry in cardiac tissue is based on a hypothesis proposed

a)Address for correspondence: Bradley J. Roth, Department of Physics and Astronomy, Vanderbilt University, Box 1807, Station B, Nashville, TN 37235.

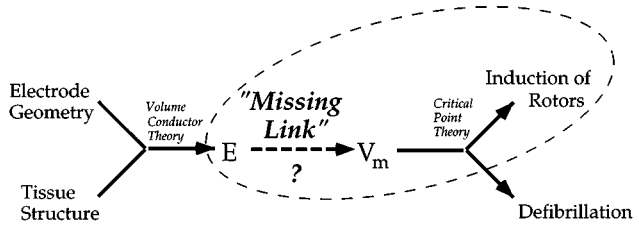

FIG. 1. The sequence of events occurring during electrical stimulation of the heart. The dashed oval encloses topics emphasized in this review.

by Winfree in 1983.[1] This hypothesis can be illustrated by considering the ''pinwheel experiment.'' [2] Suppose that a brief stimulus (S1) initiates an action potential wave front propagating from right to left through a two-dimensional sheet of cardiac tissue, as shown in Fig. 2a. The tissue is quiescent (Q) at the far left of the sheet. Excitation (E) is indicated by the dark band, and is associated with the fast upstroke of the action potential. It is followed by the plateau (P), the relatively slow repolarization (R), and then a return to quiescence. During the plateau and repolarization the tissue is refractory (shaded area). The ''critical phase'' of the cardiac action potential is the time when the application of a stimulus of appropriate strength induces reentry.[3] To a first order approximation, the critical phase occurs during the vulnerable window, near the end of the refractory period, and is denoted in Fig. 2a by a dashed line.

Now imagine that another brief electrical stimulus (S2) is applied to a point at the center of the sheet of tissue, as shown in Fig. 2b. One of the primary goals of this review is to examine how this stimulus affects the tissue. For the moment assume that the S2 stimulus depolarizes the tissue around the electrode (dot), that this depolarization falls off with distance from the electrode, and that the effect of the stimulus does not depend on direction. There exists a ''critical depolarization'' that induces reentry during the critical phase. (Winfree referred to this depolarization as the ''critical stimulus.'' [3] However, this review distinguishes between the ''stimulus''—the applied current or electric field—and the tissue response. The connection between the stimulus and the response is the missing link). The critical depolarization is indicated in Fig. 2b by the dashed circle; the hatched tissue inside the dashed circle is depolarized by an amount greater than the critical depolarization.

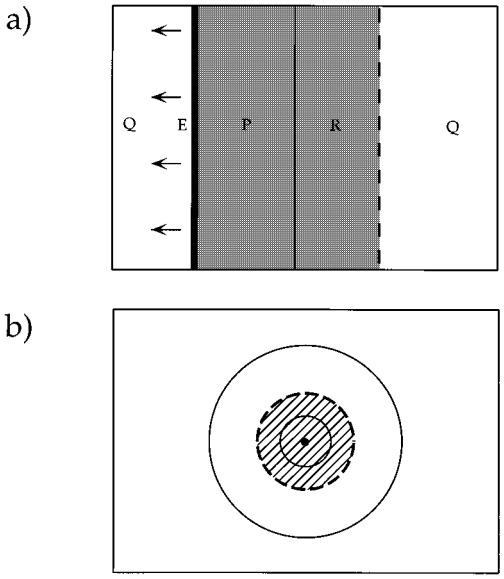

FIG. 2. (a) An action potential propagating to the left through a sheet of cardiac tissue. Q = quiescent, E = excitation, P = plateau, R = repolarization. The dashed line is the ''critical phase,'' and the shaded area represents refractory tissue. (b) Response to a point stimulus. The circles are isocontours of V_m, the dot is the electrode, the dashed circle is the ''critical depolarization,'' and the hatched area received a supracritical depolarization.

What happens if the S2 stimulus in Fig. 2b is applied as the action potential elicited by S1 is passing under the electrode? If the S2 stimulus is applied early (Fig. 3a), the tissue under the electrode is still refractory and the stimulus does

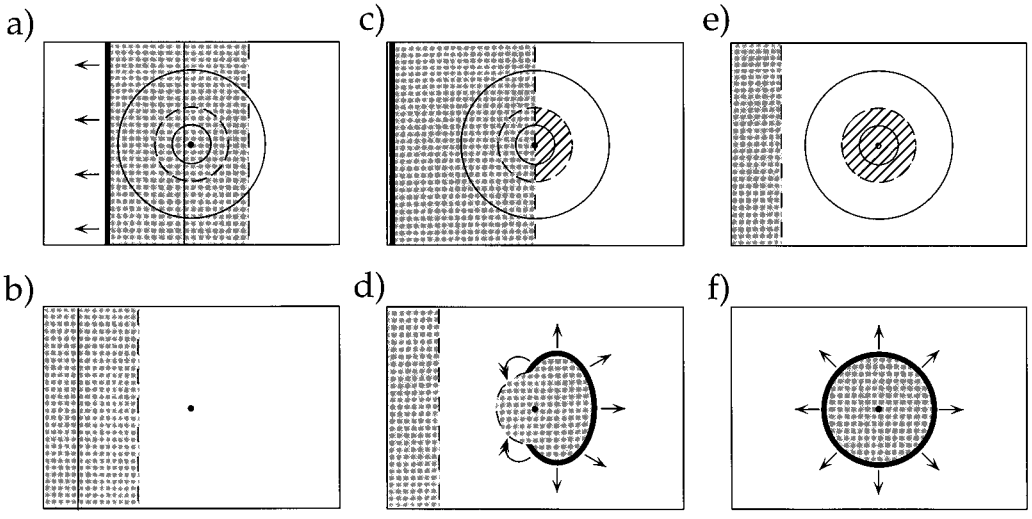

FIG. 3. The response of the tissue to an S2 stimulus applied through a point electrode (dot) at different S1-S2 intervals. The left column (a and b) represents a short S1-S2 interval, the middle column (c and d) an intermediate interval, and the right column (e and f) a long interval. The upper row (a, c, and e) shows the initial response to the stimulus, and the lower row (b, d, and f) shows the response later in time.

not excite a wave front (Fig. 3b). If the S2 stimulus is applied late (Fig. 3e), the action potential has propagated past the electrode, the tissue has recovered from refractoriness, and the stimulus initiates a closed circular wave front propagating outward (Fig. 3f). However, if the S2 stimulus is applied at an intermediate time, when the critical phase is passing nearly under the electrode (Fig. 3c), the tissue within the dashed circle on the right is excited by the stimulus. However, the tissue within the dashed circle on the left is too refractory to be excited. If the stimulus has any effect on this tissue, it would probably be to lengthen the original action potential, thereby extending its refractory period (a ''graded response''). The S2 stimulus results in the situation shown in Fig. 3d. A wave front is propagating outward, but it is not closed. It ends at the two points where the contours of critical phase and critical depolarization intersect (Fig. 3c). Winfree hypothesized that ''phase singularities'' occur at these intersections,[1] and Frazier *et al.* refer to the points of intersection as ''critical points.'' [4]

What is the fate of the wave front shown in Fig. 3d? Much of the wave front propagates outward into quiescent tissue. However, interesting wave front dynamics occurs near critical points. Since the action potential cannot propagate into the refractory tissue, at the upper critical point in Fig. 3d the wave front can propagate to the left but not down, and at the lower critical point the wave front can propagate to the left but not up. As time goes on, the tissue near the electrode finally recovers from refractoriness and becomes excitable. At this time, the wave front can propagate inward toward the stimulation site. The net result is that the wave front has traced out a spiral path; counterclockwise about the upper critical point, and clockwise about the lower critical point. Therefore, the critical points act as the pivots of spiral waves. In the cardiac electrophysiology literature, spiral waves are usually called ''rotors'' and a reentry consisting of a pair of rotors as in Fig. 3d is called a ''figure of eight'' reentry.

III. SHOCK-INDUCED TRANSMEMBRANE POTENTIAL—THE MISSING LINK

The critical point hypothesis is not only attractive theoretically, but also it has been verified in the laboratory. Shibata *et al.*[5] performed the pinwheel experiment in a dog. The heart was paced (S1) from the right ventricular outflow tract, creating a wave front propagating through the ventricles. At a selected S1-S2 coupling interval, an S2 shock was given through a cathode at the apex of the heart. Figure 4 shows an isochrone map of reentry following a 1 J shock given with a 200 ms coupling interval. Two reentrant wave fronts are present, forming a figure-of-eight pattern. When the S1 pacing was performed from the opposite side of the heart (basal portion of the left ventricle), the S1 wave front propagated in the opposite direction and the direction of rotation about the reentrant loop reversed (Fig. 9 of Shibata *et al.*).[5] These results are qualitatively consistent with the critical point hypothesis. Chen *et al.*[6] reported similar results, and acknowledged that, ''[Winfree] predicted that a pair of singularity

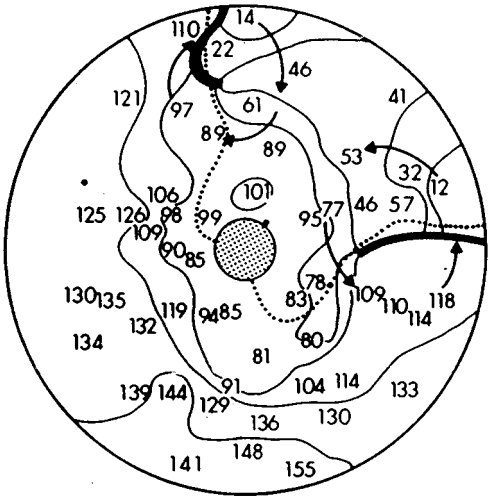

FIG. 4. Experimental evidence supporting the critical point hypothesis. The right ventricle was paced, creating an S1 wave front traveling roughly from the bottom to the top of the isochronal map. The S2 shock of 1 J was delivered 200 ms after the last pacing stimulus; the shaded circle at the center is the shock electrode. The dotted line is the location of the myocardium that activated 145 ms before the shock; if all of the ventricular myocardium had a refractory period of 145 ms, this line would represent the border between myocardium that is still refractory (top) and is not refractory (bottom) at the time of the shock. The thick line represents a region of unidirectional block. The numbers represent the location of the epicardial recording electrodes and give the time of activation after the shock, in milliseconds. *Reproduced with permission from Shibata et al., Am. J. Physiol. 255, H891–H901 (1988).*

points will be present and cause two mirror-image rotors that will form a figure-of-eight reentry pattern as we observed experimentally.''

The critical point hypothesis also inspired an experimental method for the induction of a single rotor in the heart: cross-field stimulation. In this method, two electric shocks, S1 and S2, are delivered with an appropriate delay through two line electrodes aligned perpendicular to each other.[4,7,8] Consider, for example, the study of Frazier *et al.*, who used cross-field stimulation to initiate rotors in a dog heart.[4] The region under study, a 3.4×3.4 cm portion of the right ventricle, was covered by a grid of recording electrodes. The S1 shock, delivered simultaneously from eight wires placed in a line on the right side of the grid, launched a wave front that propagated from right to left (Fig. 5a). After 191 ms, when roughly the right one-third of the tissue under the grid had recovered from refractoriness, an S2 shock was delivered from a wire mesh electrode below the grid. Figure 5b shows the electric field induced by the S2 shock. The magnitude of the field ranged from 13.6 V/cm next to the S2 electrode (bottom) to 2.7 V/cm away from it (top). Frazier *et al.* conjectured that these S1 and S2 shocks created a dispersion of physiological states in the tissue under the grid, from the direct excitation of the right part of the grid (hatched in Fig. 5c), to prolonged refractoriness (bottom left), to restored excitability (top left). The isochronal map of Fig. 5c shows that this dispersion indeed constituted a substrate for the creation of a rotor. The border between the excited and excitable regions (heavy line) gave rise to a propagating wave front. This wave front initially propagated to the left, then turned

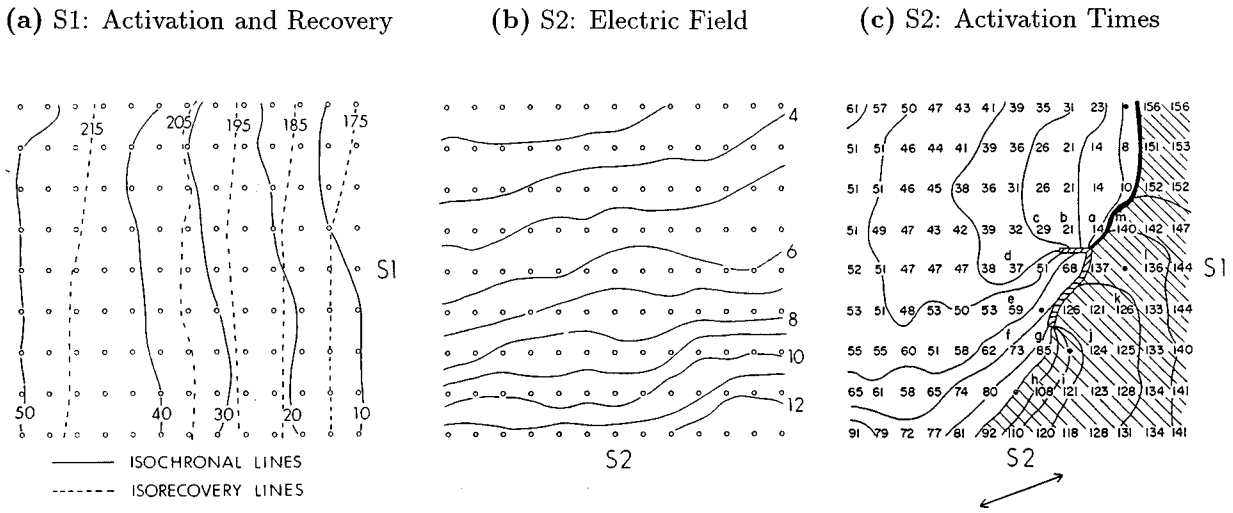

FIG. 5. The induction of rotors by cross-field stimulation. (a) The response to the S1 shock. The isochronal lines (solid) show the times when the propagating action potential was detected by the electrode. The isorecovery lines (dashed) show the time needed for the tissue to come out of the refractory period. (b) An example of an electric field induced by an S2 shock, having a strength of 150 V and a duration of 3 ms, that was delivered 191 ms after the S1 shock. The numbers shows the strength of the local field in V/cm. (c) The response to the S2 shock. The lines are isochrones and the numbers indicate local times of activation. The hatched region was directly excited by the S2 shock. The heavy line represents the border between the directly excited region and the region unaffected by S2. The arrow below the map indicates the direction of cardiac fibers. *Reproduced with permission from Frazier et al., J. Clin. Invest.* ***83****, 1039–1052 (1989).*

around and, at approximately 85 ms after the S2 shock, reentered the region directly excited by the S2 shock. It then propagated to the right and up, thereby closing a reentry loop that persisted for several revolutions.

The pinwheel experiments[5,6] and the cross-field stimulation experiments[4,7,8] provide strong support for the critical point hypothesis. Indeed, the experimental evidence is so compelling that today this hypothesis is universally referred to as the ''critical point *theory*.'' However, these experiments also exposed the missing link in our understanding of the events leading to the initiation of rotors: the precise mechanism by which the S2 shock induces the required changes in the physiological state of the tissue. For example, Fig. 4 shows that in the pinwheel experiment of Shibata *et al.*, the first post-shock excitations that gave rise to propagating wave fronts occurred 12 and 14 ms after S2 in the basal portion of the ventricles, i.e., several centimeters from the S2 electrode at the apex. Likewise, Fig. 5c shows that in the cross-field stimulation experiment of Frazier *et al.*, the first such excitation was detected 8 ms after the S2 stimulus, approximately 3.2 cm away from the S2 electrode. Where did this excitation come from? In his paper, Frazier *et al.* assumed that the S2 shock directly excited the entire right (recovered) part of the grid (hatched in Fig. 5c).

However, both Shibata's and Frazier's experiments used extracellular electrodes to record the activity of the tissue. Since extracellular recordings are contaminated with shock artifacts, a question arises whether the existence and the extent of the directly excited region can be reliably estimated from such recordings. Frazier *et al.* discusses the criteria used to identify the directly excited region and quantifies the uncertainty in estimating its extent (see p. 160 of Ref. 9). These criteria were tested by Daubert *et al.*[10] who inserted a MAP electrode in the middle of the array of extracellular electrodes and verified that the same region is classified as directly excited in both extracellular and MAP recordings. Knisley and Hill[8] performed an experiment similar to Frazier's on Langendorff-perfused rabbit hearts and used voltage-sensitive dyes to record transmembrane potential. This study confirmed some of the observations made by Frazier *et al.*, namely that the post-shock wave fronts appear first away from the electrode and that the region immediately adjacent to the electrode has its refractoriness prolonged by the shock. However, this study monitored a 0.9×0.9 cm area of tissue, much smaller than did Frazier *et al.*, and it could not give a complete record of the activation sequence immediately following the shock. In particular, the directly excited region lay outside of the monitored area, so its location and extent could not be verified. Therefore, one must look for additional evidence in recent studies that measured the change in V_m induced by the shock in regions away from the electrode.[11,12] In these studies, shocks were delivered during the plateau, so they could not cause direct excitation. Nevertheless, the observed magnitude of the change in V_m appears to be sufficient for excitation of resting myocardium, supporting the assumption that the shock can directly excite the tissue at a distance.

Another possibility is that only a small region close to the S2 electrode was excited and the action potential propagated upwards within the right part of the grid. Upon reaching the top of the grid, this wave front could have turned to the left and initiated a rotor, as seen in Fig. 5c. However, the comparison with Frazier's experiment does not support this scenario. With the propagation velocity of 0.5–0.7 m/s, it takes an action potential about 50 ms to transverse the distance of 3.2 cm. Such a propagation delay should have been detected experimentally, but it is not seen in Frazier's results. There are no propagation wave fronts starting at the S2 electrode; the isochronal map of Fig. 5c shows that the first activation was detected at 8 ms after the S2 shock, approxi-

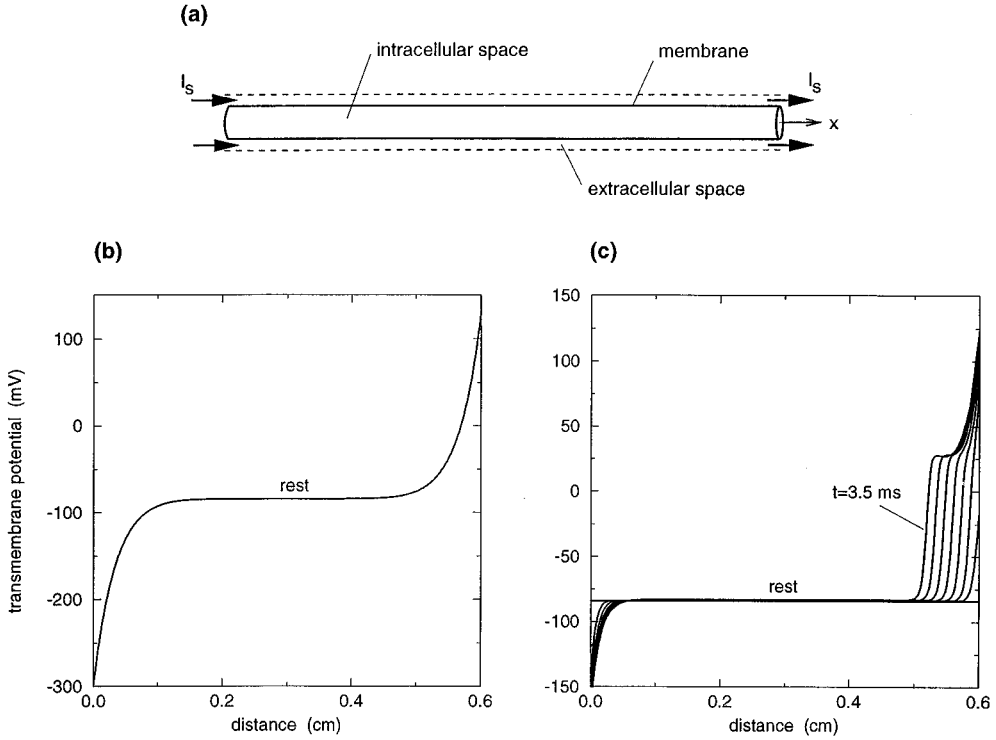

FIG. 6. (a) A one-dimensional model of a cardiac strand, stimulated with current I_s delivered through extracellular electrodes. The extracellular field established by this current is 5.7 V/cm. (b) The steady-state distribution of transmembrane potential. The membrane is assumed passive. (c) Excitation of the strand via a propagating wave front. The membrane is represented by the Luo-Rudy model.[16] The plot shows the distribution of the macroscopic transmembrane potential V_m^0 at rest and at times $t=0.5,1,\ldots,3.5$ ms.

mately 3.2 cm away from the electrode, precisely where the boundary between the excited and unaffected tissue should lie. This argument, as well as the evidence summarized in the previous paragraph, support the conjecture of Frazier *et al.* that in this experiment, the S2 shock directly excited the tissue up to several centimeters from the electrode.

How exactly this is accomplished is not known. Figure 5b follows the tradition of expressing the strength of S2 in terms of the electric field. However, the electric field is not a state variable of the cardiac membrane and, as such, it cannot directly affect its physiological state. To cause the changes in the physiological state required by the critical point theory, the shock must first change V_m. Thus, in order to completely understand the induction of rotors in these experiments, we must first address the missing link question: How does the electric field alter the transmembrane potential? To this end, the next section reviews the current state of knowledge regarding the mechanisms by which electric fields affect V_m.

IV. MECHANISMS OF THE SHOCK-INDUCED TRANSMEMBRANE POTENTIAL

A. One-dimensional cable theory

This section uses the one-dimensional cable equation[13] to introduce the most basic mechanism by which an external electric field changes the transmembrane potential: a direct polarization of the membrane by the stimulating current. The prototypical situation is shown in Fig. 6a, in which a strand of cardiac muscle of length L is stimulated by two electrodes at its ends. In accordance with common clinical and experimental practice, these are *extracellular* electrodes, i.e., they deliver a stimulating current I_s to the extracellular space. The experimental realization of this type of stimulation was performed by Weidmann in a preparation that consisted of a calf trabecular muscle strand surrounded by oil.[14]

The equations governing potentials in Fig. 6a are

$$g_i \frac{\partial^2 \phi_i}{\partial x^2} = \beta\left(C_m \frac{\partial V_m}{\partial t} + I_{\text{ion}} \right),$$
$$g_e \frac{\partial^2 \phi_e}{\partial x^2} = -\beta\left(C_m \frac{\partial V_m}{\partial t} + I_{\text{ion}} \right), \tag{1}$$

where ϕ_i and ϕ_e are potentials in the intra- and extracellular space, $V_m \equiv \phi_i - \phi_e$ is the transmembrane potential, g_i and g_e are the effective intra- and extracellular conductivities, β is the ratio of membrane surface area to tissue volume, C_m is the surface capacitance of the membrane, and I_{ion} is the ionic current density. Stimulation with extracellular electrodes is represented by the boundary conditions,

$$-g_i \frac{\partial \phi_i}{\partial x} = 0$$
$$\text{at } x = \pm L/2, \tag{2}$$
$$-g_e \frac{\partial \phi_e}{\partial x} = J_s$$

where $J_s = I_s/A$, with A denoting the total cross-sectional area of the strand (both intra- and extracellular regions). Equations (1) and (2) can each be combined into one equation that involves V_m only,

$$\frac{g_i g_e}{g_i + g_e} \frac{\partial^2 V_m}{\partial x^2} = \beta \left(C_m \frac{\partial V_m}{\partial t} + I_{\text{ion}} \right), \tag{3}$$

$$\frac{\partial V_m}{\partial x} = \frac{J_s}{g_e} \quad \text{at } x = \pm L/2. \tag{4}$$

If the external current J_s is sufficiently small, the membrane can be considered passive and the ionic current linear, $I_{\text{ion}} = V_m/R_m$, where R_m is the surface resistance of the membrane and V_m is measured with respect to its value at rest. With this simplification, the steady state solution for V_m is

$$V_m(x) = \frac{J_s \lambda}{g_e} \frac{\sinh(x/\lambda)}{\cosh(L/2\lambda)}, \quad -L/2 \leqslant x \leqslant L/2, \tag{5}$$

where

$$\lambda \equiv \sqrt{\frac{R_m g_i g_e}{\beta(g_i + g_e)}}$$

is the length constant.

This solution, plotted in Fig. 6b, shows that next to the positive electrode (the anode) the strand is hyperpolarized, and next to the negative electrode (the cathode) it is depolarized. The magnitude of V_m decays exponentially with the distance from either electrode, so if the strand is more than several lengths constants long, the magnitude of V_m in the middle is very small. Hence, this mechanism of polarization affects the strand directly only in the regions near the ends. (These regions do not have to be in the physical proximity of the electrodes. They develop wherever the current enters or leaves the tissue and the sealed-end boundary conditions (2) apply. For example, during transthoracic stimulation, the electrodes are on the chest yet they establish polarization on the surfaces of the heart). The effect of the stimulus on the rest of the strand is indirect and involves the propagation of an action potential. This scenario is illustrated in Fig. 6c,[15] in which the membrane of the strand is excitable and represented by the Luo-Rudy model.[16] The depolarized tissue near the cathode is excited directly, and the rest of the strand is excited by a propagating wave front.

B. Limitations of the one-dimensional cable theory

The steady-state solution of the cable equation, depicted in Fig. 6b, shaped the traditional understanding of how shocks affect the transmembrane potential. This mechanism is sufficient to understand cardiac pacing, when a suprathreshold but still relatively small stimulus is applied through a unipolar cathode. However, it is not adequate to explain the effects of strong electric fields, such as field stimulation, the initiation of rotors, and defibrillation. Experiments have demonstrated that strong shocks can cause a so-called ''field stimulation'' of the myocardium: the direct excitation of tissue far from the electrodes by the shock. The extent of the excited region depends on the strength of the shock and can even encompass the whole heart.[17] Likewise, the termination of ventricular fibrillation by a defibrillation shock requires that the shock affects at least a critical mass of the heart, estimated at 80%.[18] However, cable theory cannot explain how the shock alters V_m away from the electrodes.

Additional conceptual problems arise because, in cable theory, the polarity of the closest electrode determines whether the membrane is depolarized or hyperpolarized. Since the membrane responds differently to depolarization versus hyperpolarization, the response of the heart should depend strongly on the polarity of the shock. This is indeed the case for pacing with unipolar electrodes: pacing thresholds for an anode are 2-4 times larger than for a cathode.[19,20] The situation changes for large shocks. Thresholds for field stimulation are independent of polarity.[9] The response to a defibrillation shock depends on the position of the electrodes. When both electrodes are on the heart or both on the chest, the defibrillation threshold depends weakly, or does not depend at all, on the shock polarity.[21,22] When only one of the electrodes is on the heart, the defibrillation threshold is generally lower when this electrode is an anode.[23–25] However, the defibrillation threshold decreases by only 17%–33%, far less than the difference observed during pacing. Also, a significant number of patients have a lower defibrillation threshold with the reverse polarity, so the optimal polarity cannot be predicted *a priori*.[26,27]

These unresolved questions have stimulated recent modeling efforts directed toward discovering additional mechanisms by which electric shocks can alter V_m.[28,29] The resulting theoretical developments are discussed in the remainder of this section.

C. Virtual electrodes

One limitation of the cable model illustrated in Fig. 6 is that it is one-dimensional. Higher-dimensional models introduce a new property of cardiac tissue: anisotropy. The electrical conductivity of cardiac tissue is anisotropic; it is different in the direction parallel to the myocardial fibers than in the direction perpendicular to them. Consequently, in two- and three-dimensional tissue, one would expect to see a qualitatively different behavior. However, formulating a model for more than one dimension should be done with caution. A straightforward extension of the cable equation (3), assuming that the extracellular space is grounded,[30] leads to a ''monodomain'' model, consisting of a single reaction-diffusion equation. This model exhibits behavior similar to a one-dimensional cable. Polarization of the membrane occurs only in the proximity of the regions where current enters or leaves the tissue and the decay of V_m with the distance occurs at an even faster rate than in one dimension.[30–32]

The proper tool for studying effects of electric shocks on the transmembrane potential in two and three dimensions is the ''bidomain'' model,[33,34] which allows the explicit representation of the flow of current in both intracellular and extracellular domains (Fig. 7). The equations governing the intracellular and extracellular potentials,

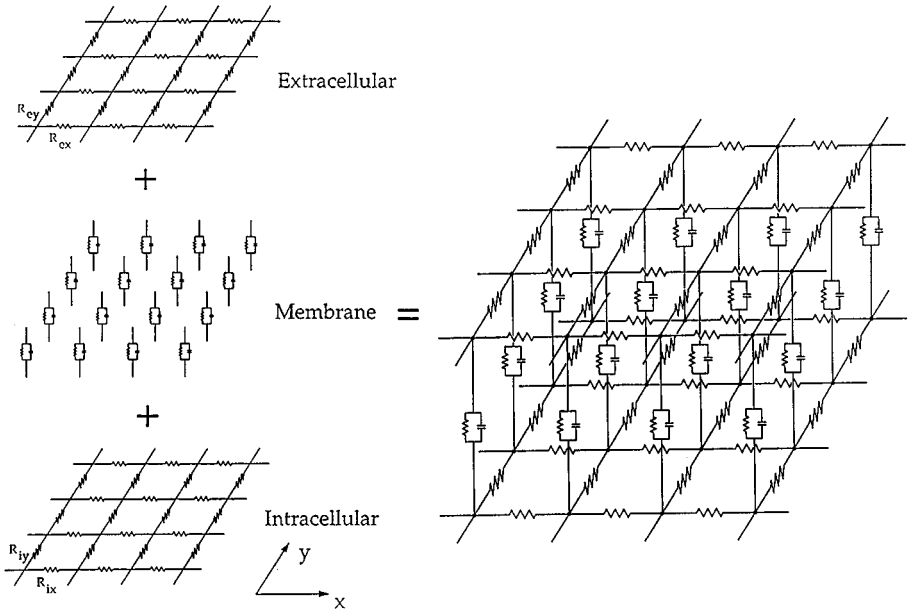

FIG. 7. The two-dimensional bidomain model. The upper and lower resistor networks represent the electrical properties of the extracellular and intracellular domains, respectively. The vertical resistors and capacitors represent the electrical properties of the membrane. The tissue is anisotropic, so the resistors parallel to the x-axis (R_{ix} and R_{ex}) are different than the resistors parallel to the y-axis (R_{iy} and R_{ey}). The tissue has unequal anisotropy ratios if $R_{ix}/R_{iy} \neq R_{ex}/R_{ey}$. *Reproduced with permission from Saypol and Roth, J. Cardiovasc. Electrophysiol.* ***3****, 558–566 (1992).*

$$\nabla \cdot (\tilde{g}_i \nabla \phi_i) = \beta \left(C_m \frac{\partial V_m}{\partial t} + I_{\text{ion}} \right),$$
$$\nabla \cdot (\tilde{g}_e \nabla \phi_e) = -\beta \left(C_m \frac{\partial V_m}{\partial t} + I_{\text{ion}} \right), \tag{6}$$

are generalizations of Eqs. (1). The intracellular and extracellular conductivity tensors, $\tilde{g}_i$ and $\tilde{g}_e$, represent the anisotropic electrical properties of cardiac tissue. The tilde in the symbols $\tilde{g}_i$ and $\tilde{g}_e$ indicates that the conductivities are tensors, or matrices, in contrast to the scalar variables g_i and g_e in (1). In the intracellular space, the ratio of conductivities parallel and perpendicular to the fibers is about 10; in the extracellular space, the ratio is about 2.5.[35] This condition is called ''unequal anisotropy ratios'' and leads to many interesting and surprising predictions of the bidomain model.[36]

One unexpected result of the bidomain model was obtained in 1989 by Sepulveda *et al.*[37] Their study simulated a two-dimensional sheet of cardiac tissue using the bidomain model with unequal anisotropy ratios and a passive membrane. When a steady current was applied through a unipolar, extracellular cathode, a region of depolarized tissue formed directly under the cathode, similar to what would be expected from a monodomain model. However, regions of hyperpolarization developed 1-2 mm away from the cathode in the directions parallel to the myocardial fibers (Fig. 8). These hyperpolarized regions are not near an anodal electrode, and are therefore called ''virtual anodes.'' If the stimulating electrode is an anode rather than a cathode, the tissue is hyperpolarized under the anode but depolarized a few millimeters away from the anode along the fiber direction at the ''virtual cathodes.'' [37] Virtual electrodes were unexpected because they have no analogs in one-dimensional cable theory,[14] in the monodomain model,[30] or in the bidomain model with equal anisotropy ratios.[38] However, similar regions of reversed polarity have been observed during stimulation of a nerve axon by an extracellular electrode located in the surrounding volume conductor,[28] and existence of such regions is predicted from approximate analytical solutions of the bidomain equations.[39]

In 1995, three groups verified experimentally the existence of adjacent areas of depolarization and hyperpolarization around a unipolar electrode.[40–42] Each group recorded V_m optically using transmembrane potential-sensitive fluorescent dyes. Figure 9 contains data from Wikswo *et al.*[42]

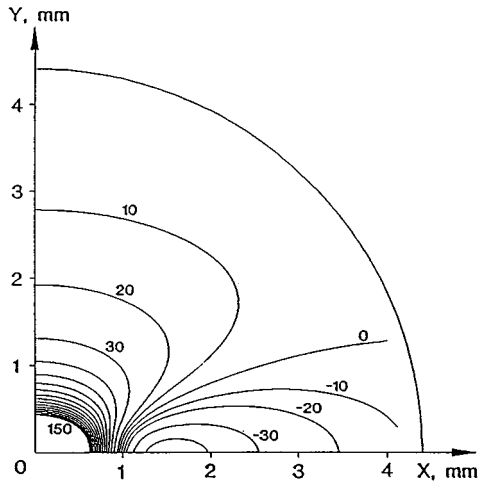

FIG. 8. The calculated steady-state V_m established by an extracellular point source in a passive, two-dimensional bidomain. The cathode is located at the origin. Only one quadrant of the x-y plane is shown. The myocardial fibers are oriented parallel to the x-axis, and the tissue has unequal anisotropy ratios. Contour lines are drawn every 10 mV. *Reproduced with permission from Sepulveda et al., Biophys. J.* ***55****, 987–999 (1989).*

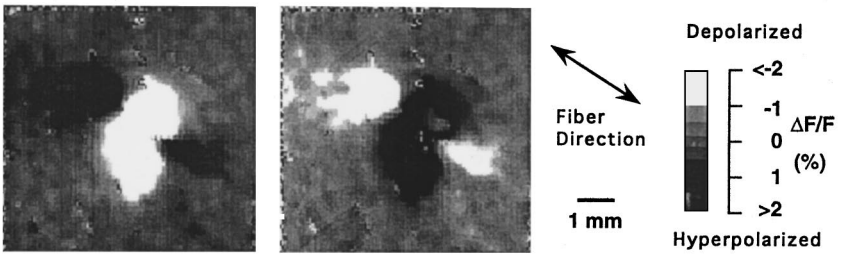

FIG. 9. Gray-scale images of V_m associated with injection of current into refractory cardiac tissue. (a) The image for a 10 mA, 2 ms cathodal S2 applied through a point electrode. The fiber orientation is from lower right to upper left. The bar shows the fractional change in fluorescence. (b) The image for a 10 mA, 2 ms anodal S2 stimulation at the same location. *Reproduced with permission from Wikswo et al., Biophys. J.* ***69****, 2195–2210 (1995).*

showing virtual electrodes appropriately positioned along the fiber direction. These data provide convincing evidence in support of the bidomain model.

Virtual electrodes provide a consistent theoretical framework to explain four different mechanisms of stimulation occurring in cardiac tissue. Dekker observed that the excitation can be triggered by the onset of either a cathodal or anodal pulse (''cathode make'' and ''anode make'') or by the end of a pulse of either polarity (''cathode break'' and ''anode break'').[20] Cable theory can explain only cathode make stimulation (Fig. 6c). Virtual cathodes arising during anodal stimulation explain anode make stimulation: if the depolarization at a virtual cathode reaches threshold, a wave front is initiated.[28] Numerical simulations and experiments indicate that break stimulation is caused by an interaction of virtual electrodes surrounding a real electrode.[42,43] This interaction is especially important when the stimulus is delivered to refractory tissue. For example, consider an anodal S2 stimulus applied near the end of the S1 refractory period. The depolarization at the virtual cathode does not trigger an action potential because, when the S2 stimulus turns on, the tissue is still refractory from the S1 action potential. However, during the S2 pulse the strong hyperpolarization under the anode removes any inactivation of the sodium channels and renders the tissue there excitable. When the S2 stimulus turns off, the depolarization at the virtual cathode diffuses into the hyperpolarized tissue under the anode and excites it, resulting in anode break stimulation. A similar mechanism underlies cathode break stimulation.

D. Changing fiber orientation

When Sepulveda *et al.*[37] used the bidomain model to study unipolar stimulation, they assumed a constant direction of the cardiac fibers. Since V_m predicted in their study is significant only within a few millimeters around the electrode, their assumption is reasonable: over a millimeter spatial scale the fiber orientation in the heart is nearly uniform. But over the scale of the entire heart, the fiber geometry is extraordinarily complex.[44] Fibers curve to conform to the shape of the ventricular wall, and change direction with the depth across the wall. If anisotropy is important during field stimulation, the detailed fiber geometry may influence how the heart responds to a shock.

In fact, the curvature of fibers in the heart provides another mechanism for the shock-induced transmembrane potential. In order to understand why, consider again the one-dimensional cable model of Weidmann[14] (Fig. 6). At the ends of the strand, the current is entirely extracellular (the intracellular space is sealed). But over a distance of a few length constants, the current redistributes between the intra- and extracellular spaces proportionally to their respective conductivities. Except near the ends of the strand, the gradients of intracellular and extracellular potentials are equal.

A similar situation may occur during stimulation of the whole heart. If the fibers lie parallel to an applied electric field, current will distribute between the intracellular and extracellular space according to the longitudinal (L) intracellular and extracellular conductivities. If these conductivities are equal ($g_{eL}=g_{iL}$),[35] then half of the current is intracellular and half extracellular (Fig. 10). Now, suppose the fibers curve by 90° throughout a region in which the applied electric field maintains a fixed strength and direction. In this case, the current will redistribute according to the transverse (T) intracellular and extracellular conductivities. In the direction perpendicular to the fibers, the extracellular space of cardiac tissue has a conductivity about four times larger than the intracellular space ($g_{eT}=4g_{iT}$),[35] so 4/5 of the current will be in the extracellular space and 1/5 in the intracellular space. Therefore, as the fibers curve from being parallel to the applied field to being perpendicular to it, 30% of the current must move from the intracellular space to the extracellular space (Fig. 10). The only way this can occur is for

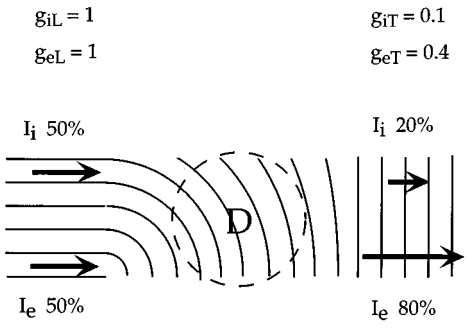

FIG. 10. A schematic drawing illustrating how fiber curvature can polarize cardiac tissue. The curving lines show the fiber direction. On the left, the applied electric field is parallel to the fibers, so that half the current is intracellular and half extracellular (arrows). On the right, the fibers are perpendicular to the applied electric field, so 20% of the current is intracellular, and 80% extracellular (arrows). The region inside the dashed circle labeled 'D' indicates an area of depolarization.

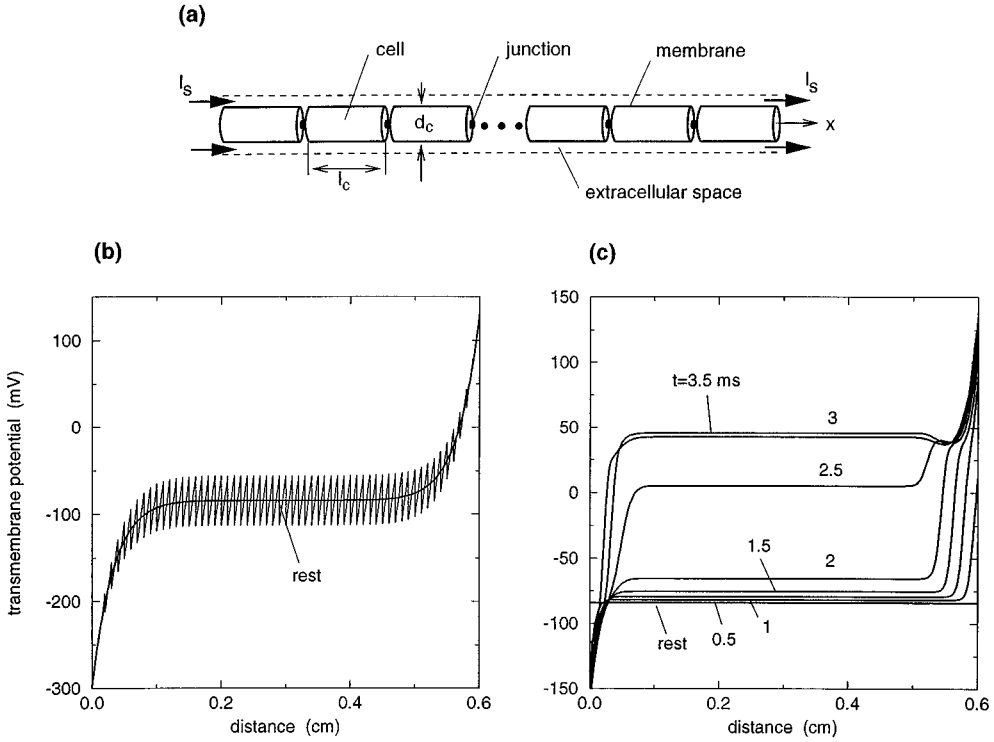

FIG. 11. (a) A one-dimensional model of a cardiac strand consisting of individual cells. Each cell has a cylindrical shape and the black dot on its face indicates the location of a low-resistance connection with a neighboring cell. The extracellular space forms a cylindrical layer surrounding the strand. This strand is stimulated with current I_s delivered through extracellular electrodes. The extracellular field established by this current is 5.7 V/cm. (b) The steady-state distribution of the transmembrane potential. The membrane is assumed passive. The two lines in the plot are the macroscopic transmembrane potential V_m^0 (smooth line) and the total transmembrane potential Φ_m, which contains both V_m^0 and the sawtooth potential V_m^1. (c) Field stimulation of the discrete cardiac strand. Here, the membrane is represented by the Luo-Rudy model.[16] The plot shows the distribution of the macroscopic transmembrane potential V_m^0 at rest and at time instants $t=0.5,1,\ldots,3.5$ ms.

the current to exit the intracellular space through the membrane, depolarizing it. Similarly, if the fibers change direction toward the applied field, the tissue is hyperpolarized. Polarization will occur whenever the ratio of intracellular and extracellular conductivities depends on direction, $g_{iL}/g_{eL} \neq g_{iT}/g_{eT}$, which is equivalent to the condition of unequal anisotropy ratios, $g_{iL}/g_{iT} \neq g_{eL}/g_{eT}$.

The above scenario was tested numerically by Trayanova *et al.*,[45] who developed a model of cardiac stimulation that incorporated fiber curvature but used an idealized geometry. In this model, the heart was represented as a spherical shell, with the myocardial fibers aligned along lines of longitude (using an analogy with a globe). The model predicted a large polarization of the tissue at the inner and outer surfaces of the heart, analogous to the polarization of a one-dimensional strand at its ends (Fig. 6b). However, deep in the tissue the field created a weaker, diffuse polarization whose magnitude correlated with the fiber curvature. This weak polarization may play a role during stimulation with strong electric fields, such as during reentry induction or defibrillation. The model of Trayanova *et al.* used a rather large radius of curvature of the fibers (greater than or equal to 3 cm). In a real heart, the radius of curvature varies and in many regions may be much less than 3 cm, creating a stronger polarization than Trayanova *et al.* predicted. Given the complicated fiber geometry within the heart, a uniform applied electric field may produce a complex distribution of V_m (see Fig. 5 in the article by Trayanova *et al.* in this issue).[46]

E. Cellular-level discontinuities

The mechanisms for the shock-induced transmembrane potential discussed in previous sections are based on a continuum representation of the myocardium. Their effects occur on a macroscopic scale: over distances of a length constant, typically 0.3-1 mm,[47] or larger. This section describes a mechanism that accounts for the distribution of V_m on the scale of a single cell, whose typical dimensions are $20\times 100\ \mu$m.[48]

Figure 11 shows a prototypical situation in which cellular-level changes in V_m arise. Again, we consider a one-dimensional strand of cardiac muscle of length L, stimulated by two extracellular electrodes at its ends. However, in contrast to the continuous strand of Fig. 6, this strand is composed of discrete cells of length l_c and diameter d_c that are abutted end-to-end and connected electrically by gap junctions. The mathematical description of potentials arising in such a strand can be obtained via homogenization theory.[49] Assuming that the structure of the strand is periodic in space, we can treat the potentials as functions of two spatial variables, macroscopic x and microscopic y. The dependence on y is periodic, with the period equal to the length of the cell,

l_c. The total transmembrane potential Φ_m is represented, to a leading order, by a two-term expansion,

$$\Phi_m(x,y) = V_m^0(x) + V_m^1(x,y),$$
$$-L/2 \leqslant x \leqslant L/2 \quad \text{and} \quad -l_c/2 \leqslant y \leqslant l_c/2, \tag{7}$$

in which V_m^0 reflects the changes in the transmembrane potential occurring on the macroscopic spatial scale and V_m^1 reflects the changes caused by the polarization of individual cells. (This expansion, as well as other equations in this paper, is written in the dimensional form. Hence, in contrast to the previous publication,[49] the small parameter does not appear.)

The macroscopic component V_m^0 is governed by a discrete-fiber counterpart of the one-dimensional cable equation, Eq. (3)

$$\frac{g_i g_e}{g_i + g_e} \frac{\partial^2 V_m^0}{\partial x^2} = \beta \left(C_m \frac{\partial V_m^0}{\partial t} + i_{\text{ion}} \right). \tag{8}$$

The difference between the models for the continuous and the discrete strands is that the right hand side of Eq. (3) contains I_{ion}, the ionic current of the space-clamped membrane, whereas Eq. (8) contains i_{ion}, the *macroscopic* ionic current, defined as a surface average of I_{ion} over the membrane M of a cell,

$$i_{\text{ion}} \equiv \frac{1}{S} \int_M I_{\text{ion}}(\Phi_m)\, da, \tag{9}$$

where S is the membrane surface area. Note that in Eq. (9), the ionic current I_{ion} at any point on the membrane depends upon the total transmembrane potential Φ_m, indicating that the evolution of the macroscopic transmembrane potential V_m^0 can be caused by V_m^0 itself, by V_m^1, or by a combination of both.

The microscopic component V_m^1 is determined by

$$V_m^1(x,y) = E(w_i(y) - w_e(y)), \tag{10}$$

where

$$E \equiv J_s/(g_i + g_e) \tag{11}$$

approximates the extracellular field established in the center of the strand by the stimulating current J_s. In Eq. (10), w_i, w_e are weight functions that depend on the geometry of the individual cells. For the strand of Fig. 11a, in which all cells have the shape of a thin cylinder, the weight functions can be approximated as[15]

$$w_i = y \quad \text{and} \quad w_e = 0, \quad -l_c/2 \leqslant y \leqslant l_c/2. \tag{12}$$

Hence, the microscopic potential V_m^1 changes linearly within the cell, and its slope is proportional to E

$$V_m^1(x,y) = Ey, \quad -l_c/2 \leqslant y \leqslant l_c/2. \tag{13}$$

At the end of each cell, y changes from $-l_c/2$ to $l_c/2$ and V_m^1 has a jump of magnitude El_c. The right hand side of Eq. (13) indicates that V_m^1 is independent of the macroscopic variable x. This is true only for the one-dimensional cable equation in which the electric field E is constant. In two and three dimensions, a dependence of V_m^1 on x arises because E varies with position.

Two examples illustrate the influence of the cellular structure of the myocardium on the shock-induced transmembrane potential. The first one presents the steady-state solution for the transmembrane potential in a discrete strand. As in Sec. IV A, this solution is computed under the simplifying assumption of a passive membrane, $I_{\text{ion}} = \Phi_m / R_m$. The macroscopic ionic current, evaluated from Eq. (9), is

$$i_{\text{ion}} = \frac{1}{\pi d_c l_c} \int_{-l_c/2}^{l_c/2} \int_0^{2\pi} \frac{V_m^0 + Ey}{R_m} \frac{d_c}{2} d\theta\, dy = \frac{V_m^0}{R_m}. \tag{14}$$

For a linear I_{ion}, the macroscopic ionic current does not contain a contribution from V_m^1. Consequently, the right hand side of Eq. (8) is the same as the right hand side of Eq. (3) and V_m^0 is the same as V_m computed in Sec. IV A and given by Eq. (5). With V_m^1 determined by Eq. (13), the total transmembrane potential is

$$\Phi_m(x,y) = \frac{J_s \lambda}{g_e} \frac{\sinh(x/\lambda)}{\cosh(L/2\lambda)} + Ey, \tag{15}$$

where $-L/2 \leqslant x \leqslant L/2$ and $-l_c/2 \leqslant y \leqslant l_c/2$. Figure 11b shows that away from the directly polarized ends of the strand the transmembrane potential has a characteristic ''sawtooth'' appearance: The ends of the cells facing the cathode are depolarized and the ends facing the anode are hyperpolarized. Hence, in the literature, the transmembrane potential induced by the polarization of individual cells is commonly referred to as the ''sawtooth potential.''

The passive, steady-state solution of Fig. 11b illustrates the sawtooth potential but not its effect on the physiological state of the strand. Note that the macroscopic ionic current i_{ion}, when evaluated with a linear I_{ion}, does not contain any component coming from the sawtooth potential. A second example, which uses a nonlinear model of the membrane, demonstrates the ability of the sawtooth to affect the physiological state. Figure 11c illustrates field stimulation of the discrete strand via the sawtooth mechanism. The strand, whose membrane is represented by the Luo-Rudy model,[16] is stimulated with an external current I_s large enough to establish an electric field of 5.7 V/cm. As shown in Fig. 11b, this field polarizes the cells of the strand, causing a sawtooth potential of the magnitude $\pm$ 28.5 mV (computed from (13) as one half times the cell length, 100 μm, times the field strength). But in a nonlinear model, the depolarization and hyperpolarization at each end of the cell do not necessarily result in equal and opposite ionic current. If the shock is applied to the tissue at rest, then the sawtooth potential opens sodium channels at the depolarized end of each cell, allowing an inward flow of sodium current. This current is much larger than outward currents flowing in other parts of the membrane, so it drives the potential of each cell towards depolarization, leading to the direct excitation of almost the entire strand (Fig. 11c).[15]

The sawtooth potential provides an elegant theoretical explanation for the experimental observations related to field stimulation and defibrillation. First, Eq. (13) indicates that the magnitude of the sawtooth is proportional to the electric field, explaining the experimental finding that the success or failure of stimulating and defibrillating shocks depends on

the strength of the electric field.[9,50,51] Second, in contrast to the macroscopic transmembrane potential that decays to zero away from the electrodes, the electric field retains an appreciable magnitude throughout most of the heart.[52–54] Hence, the sawtooth appears be capable of having a truly *direct* effect on the entire heart. Finally, the sawtooth potential affects each cell in the same way, depolarizing one half and hyperpolarizing the other. It can therefore explain the relative insensitivity of the thresholds for field stimulation and defibrillation to the polarity of the electrodes.[21] As a consequence, the sawtooth potential has been invoked as a mechanism of field stimulation and defibrillation.[55–61]

However, the sawtooth hypothesis lacks direct experimental confirmation. All evidence supporting the role of the sawtooth potential in field stimulation and defibrillation is indirect and based on qualitative similarities between theoretical and experimental results. The sawtooth potential was observed in isolated single cells,[62–64] but not in multicellular tissue *in vitro*, even when examined with sufficient spatial resolution to detect cellular events.[65,66]

V. INITIATION OF REENTRY BY UNIPOLAR STIMULATION

The previous section discussed several possible mechanisms by which an applied electric field might generate a transmembrane potential. Now we are ready to address a second question: Given a particular experiment in which reentry is initiated, can we determine the mechanism responsible for the generation of V_m? This question forces us to reconcile Winfree's critical point hypothesis with the various mechanisms of electric stimulation. We consider two different experimental conditions of reentry initiation: successive stimulation through a unipolar electrode (this section) and cross-field stimulation (next section).

In the pinwheel experiment described in Sec. II, a pair of rotors was induced by applying two successive stimuli, S1 and S2, from two different locations. Now, suppose that both S1 and S2 are applied through the same unipolar electrode. Let us assume as in Fig. 3 that the S1 critical phase contour and the S2 critical stimulus contour are both circles centered at the origin. Because two concentric circles never intersect, the critical point theory predicts that reentry cannot occur. Yet Matta *et al.*[67] performed this experiment in a dog heart, applying both S1 and S2 through a single unipolar cathode, and initiated reentry. How?

Keener[68] has suggested one answer to this puzzle: the discrete nature of cardiac tissue causes the safety factor to be reduced in the direction parallel to the fibers. Therefore, after a premature shock propagation may fail parallel to the fibers yet succeed perpendicular to them, creating the necessary unidirectional block that leads to reentry. Keener cites the experiments by Spach *et al.*[69] as evidence supporting this hypothesis. However, subsequent publications by Spach *et al.*[70] reported that block parallel to the fibers but not perpendicular to them only occurs when the tissue has ''nonuniform anisotropy'' (irregular and fractionated extracellular electrograms), and not ''uniform anisotropy'' (smooth extracellular electrograms). The induction of reentry can occur in tissue having smooth extracellular electrograms, so the effects of discrete cardiac structure on propagation do not appear to be essential for reentry, although they may be a contributing factor in some cases. Likewise, the interaction of a wave front with anatomical obstacles, such as veins and arteries, or with the ischemic region, discussed in two other articles in this issue,[71,72] cannot explain reentry occurring in a normal tissue free of macroscopic obstacles.

Another possible explanation for the reentry in such a tissue arises through the bidomain model. Anisotropy is the key to this paradox, but the explanation is more subtle than simply recognizing that in anisotropic tissue the critical phase and critical stimulus contours are ellipses rather than circles. If the two contours are concentric ellipses with the same eccentricity, they still cannot intersect. Winfree provided an important insight when he noted that the intracellular and extracellular spaces have unequal anisotropy ratios. He conjectured that this property may give the critical phase and critical stimulus ellipses different eccentricities, so that they would intersect at four locations and would induce four spiral waves.[73] Subsequent studies have clarified this issue by showing that the S2 critical stimulus contour is not an ellipse, but instead has an altogether different shape than the S1 critical phase contour. Specifically, the bidomain model implies that the S2 contour (here interpreted as a contour corresponding to the critical depolarization) has a complicated, ''dog-bone'' shape (Fig. 8), which separates a region of depolarization under the cathode from regions of hyperpolarization 1-2 mm away along the fiber direction.

Numerical studies have shown that the mechanism of reentry following successive stimulation can be explained in detail by the bidomain model with unequal anisotropy ratios.[74,75] Figure 12 shows contour plots of V_m as a function of z (parallel to the fibers) and r (perpendicular to the fibers) at several time instants after the S1 stimulus (given in milliseconds for each frame). In this calculation, the Beeler-Reuter model[76] is used to represent the dynamics of the active ion channels. The S1 stimulus is applied at $t=0$ (not shown). The contours of repolarization of the S1 action potential are shown for $t=280$ ms, just before a 20 ms cathodal S2 stimulus pulse. At $t=300$ ms, the distribution of V_m around the electrode resembles that in Fig. 8: depolarization under the electrode, hyperpolarization along the fiber axis at the virtual anode. Excitation does not occur following the start of the pulse because the tissue is still refractory, but the hyperpolarization at the virtual anode causes the tissue there to quickly recover from refractoriness. After the end of the S2 pulse, the depolarization under the cathode diffuses into the tissue at the virtual anode and excites it, a mechanism identical to a ''cathode break'' discussed in Sec. IV C. The resulting action potential can propagate only along the fiber direction, because only this tissue had its refractory period shortened by hyperpolarization. Thus, by $t=360$ ms a broken wave front is present, which develops into a spiral wave front by $t=380$ ms. Clearly, reentry occurs in this example, as the wave fronts for $t=340$ ms and $t=420$ ms are similar. An analogous mechanism occurs for anodal reentry, but the spiral wave changes direction when the stimulus changes polarity. Measurements with voltage-sensitive dyes by Lin

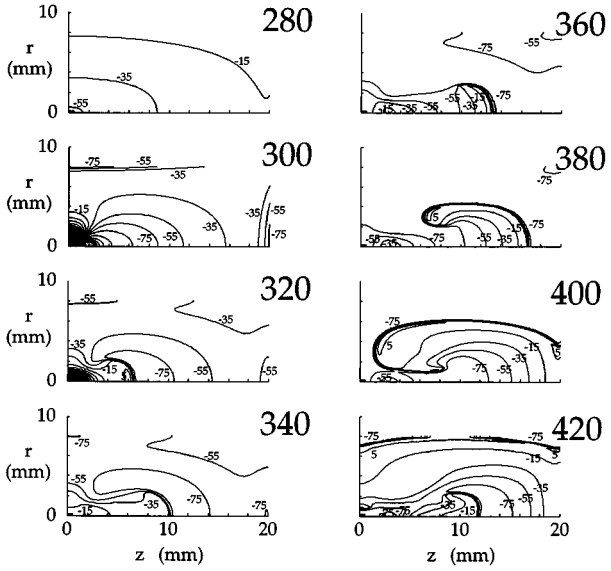

FIG. 12. Wave front dynamics following a cathodal, 20 ms S2 pulse. The S1-S2 interval was 280 ms and the S2 strength was 20 mA. Contours of V_m are plotted as functions of z (parallel to the fibers) and r (perpendicular to the fibers). The electrode is located at the origin (black rectangle, bottom left corner in each panel). Contour lines are drawn in increments of 20 mV. Depolarization greater than 145 mV is shown by dark shading; hyperpolarization greater than -215 mV is shown by light shading. The large number in each panel is the time in milliseconds. *Reproduced with permission from Roth, J. Cardiovasc. Electrophysiol.* ***8****, 768–778 (1997).*

et al.[77] provide a direct experimental verification for this mechanism of reentry induction.

The reentry shown in Fig. 12 represents a successful synthesis of the bidomain model of unipolar stimulation and critical point theory. The transmembrane potential distribution at $t=280$ ms indicates that isocontours of recovery from the S1 action potential are ellipses with their long axis parallel to the fiber direction. The S2 depolarization isocontours at $t=300$ ms, however, have ''dog-bone'' shapes, with their long axes perpendicular to the fiber direction. Thus, Winfree's conjecture of two ellipses with different eccentricities is essentially correct, although it oversimplifies the rather complicated shape of the S2 critical stimulus contour. In addition, studies using the bidomain model have exposed a new element, namely the influence of virtual anodes, which restore excitability to hyperpolarized regions of tissue. Virtual anodes create islands of excitable tissue through which wave fronts can propagate.

VI. INITIATION OF REENTRY BY CROSS-FIELD STIMULATION

A. Analysis of individual mechanisms

The analysis of the experiment of Frazier *et al.*,[4] presented in Sec. III, demonstrated that in order to fully understand the initiation of rotors by cross-field stimulation, we must determine the mechanism by which the S2 shock directly excites tissue up to 3.2 cm away from the electrode. This section starts with an assessment of which, if any, of the mechanisms described in Sec. IV can be responsible for such a direct excitation.

1. One-dimensional cable theory

The mechanism based on the one-dimensional cable theory (Sec. IV A) is not a likely explanation for cross-field stimulation. Recall that the magnitude of the transmembrane potential induced by this mechanism falls off at least exponentially with the distance from the electrode. If the length constant of cardiac tissue is approximately 1 mm[47] and if the excitation threshold of cardiac membrane is 25 mV, then in order to excite tissue 3.2 cm away from the electrode, V_m near the electrode must be on the order of 10^{12} V. This value exceeds by 12 orders of magnitude the largest transmembrane potential that a biological membrane can withstand! Experiments have shown that V_m in the range of 0.5–1 V causes electroporation of the membrane,[78–80] i.e., it creates microscopic pores across the membrane that provide nonspecific pathways for the flow of ions. During strong shocks, these pores allow a portion of the external current to flow directly into the intracellular space. In consequence, the maximum magnitude of the shock-induced V_m is limited to the threshold for electroporation, 0.5–1 V.[81] Assuming that V_m under the electrode is 1 V, 3.2 cm away its value drops to 10^{-11} mV, well below any physiological significance. Therefore, a mechanism based on cable theory cannot be responsible for the direct excitation of distant tissue by the S2 shock.

2. Virtual electrodes during unipolar stimulation

The existence of virtual anodes and cathodes around a unipolar electrode (Sec. IV C) does not explain cross-field stimulation because the spatial extent of the transmembrane potential induced by this mechanism is subject to similar limitations as cable theory. While the fall-off of the shock-induced V_m is slower than in a cable model, a physiologically significant magnitude of V_m occurs within only a few millimeters from the electrode.[37] Therefore, even at very high shock strengths, the tissue 3.2 cm away from the electrode is expected to be outside of the direct influence of the S2 shock.

3. Changing fiber orientation

The changing direction of cardiac fibers, which underlies the third mechanism (Sec. IV D), can come from three sources: the gross curvature of the heart, the in-plane rotation of epicardial fibers, and the change in fiber direction from epicardium to endocardium (i.e., from the exterior to the interior surface of the heart). The role of the curvature has been studied by Trayanova *et al.*[45] in a model of a spherical heart. As discussed in Sec. IV D, V_m retains a nonzero magnitude throughout the heart wall. Extrapolating from the results shown in Fig. 5b of the referenced work,[45] one expects that V_m induced by a 2.7 V/cm field will be approximately 12 mV. While it is almost half of the value needed for excitation, this value is only an approximation. A more realistic model, which would take into account the coupling between fibers, stimulation with a line electrode rather than a uniform field, and the decrease in the curvature due to the presence of the sielastic plaque holding the electrodes, would yield a smaller value. On the other hand, the radius of curvature in

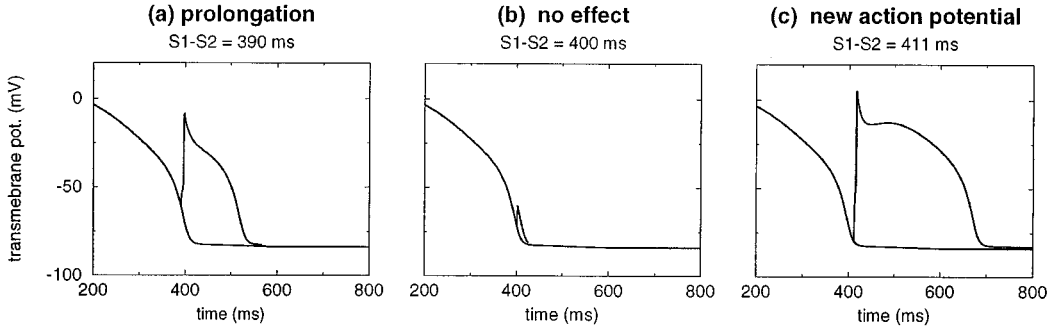

FIG. 13. Three types of response of a single cell to weak shocks: (a) prolongation of an action potential, (b) virtually no effect, and (c) new action potential. The S2 shock had the strength of twice diastolic threshold. This simulation, described in detail in Ref. 82 used the Luo-Rudy model,[16] in which the duration of an action potential is approximately 400 ms. Hence, the S1-S2 intervals are longer than in experiments.

some parts of a heart is likely to be smaller than 3 cm assumed in the model, resulting in a larger value. Therefore, the curvature of the heart can be a contributing factor to the direct excitation of the distant tissue.

The in-plane rotation of epicardial fibers is, in the animal from which the data of Fig. 5 were collected, rather small: The fibers deviate only by $\pm 5°$ from their average angle of 24°. A more detailed examination of this area of the canine heart, performed by the same author in a different study,[9] shows that there is no definitive trend in the change of fiber direction: The angle decreases in some areas and increases in others. Hence, the in-plane rotation of epicardial fibers is expected to have a negligible contribution to the shock-induced V_m.

In contrast, as one moves from epi- to endocardium, the average direction of the fibers changes by about 50° (see Fig. 9 in Frazier *et al.*[4]). If this change were responsible for the direct excitation of the distant tissue, then the position of the directly excited region should vary with the depth. However, Fig. 9 in Frazier *et al.*[4] shows that the position and extent of the directly excited region, the site and the timing of the earliest excitation, and the initial direction of propagation, measured at three planes parallel to the epicardium, are very similar. Hence, the rotation of fibers with the depth does not appear to be a factor in the direct excitation of the distant tissue. Nevertheless, one should keep in mind that this assessment pertains only to the right ventricular outflow tract of the dog heart. In a different part of the heart or in a different species, the in-plane or in-depth rotation of cardiac fibers may be of consequence.

4. Cellular-level discontinuities

The polarization of cardiac cells by the external field (Sec. IV E) appears, at a first glance, the most likely explanation for field stimulation. The sawtooth mechanism has a truly direct effect on the tissue away from the electrodes (Fig. 11c) and it provides the connection between the magnitude of the transmembrane potential and the electric field (Eq. (13)), justifying the use of the electric field as a measure of the strength of the shock. However, a closer examination reveals that in the range of fields used in Frazier's experiment, the sawtooth is too small to have the desired effect. In tissue 3.2 cm away from the electrodes, the field strength is 2.7 V/cm; with an average fiber orientation of 24°, the longitudinal and transverse field components are 1.1 and 2.5 V/cm, respectively. Assuming that cardiac cells are 100×20 μm,[48] V_m induced by these components are 5.5 and 2.5 mV, respectively. Hence, the maximum magnitude of V_m is 8 mV, which is about one-third of the excitation threshold of the cardiac membrane.

Apart from the insufficient magnitude of V_m, shocks applied during the refractory period cause the changes in the physiological state of the cell that are incongruous with Frazier's experiment and with the requirements of the critical point theory. In particular, the polarized cell responds in a qualitatively different way to weak shocks. Figure 5c suggests that weak shocks should elicit two types of responses: they should either directly excite the tissue (hatched region) or leave the tissue unaffected and ready to support a propagating action potential. However, computer simulations[82] have shown that polarized cells experience *three* types of responses: direct excitation at sufficiently long coupling intervals, virtually no effect at shorter intervals, and a considerable prolongation of an action potential at yet shorter intervals. Figure 13 shows that for the S2 shock of twice diastolic threshold, the unaffected region is very small: Only 21 ms separates coupling intervals at which S2 causes direct excitation from intervals at which S2 prolongs an action potential. In the cross-field stimulation experiment, 21 ms would correspond to approximately 1 cm. Thus, if the sawtooth were the primary mechanism, the action potential initiated at the border between the directly excited and nonexcited tissue would have propagated through only 1/4 of the region monitored in Frazier's experiment (Fig. 5) before running into tissue with prolonged refractoriness. Here, the action potential either would have blocked or its speed would have decreased dramatically. No evidence of a block or a decrease in speed is seen in Fig. 5c. Therefore, even if rotors could be started via the sawtooth mechanism, as suggested by other researchers,[83] the site of the first post-shock excitation that gives rise to a propagating wave front and the initial direction this propagation would be different than observed in the cross-field simulation experiment of Frazier *et al.*[4]

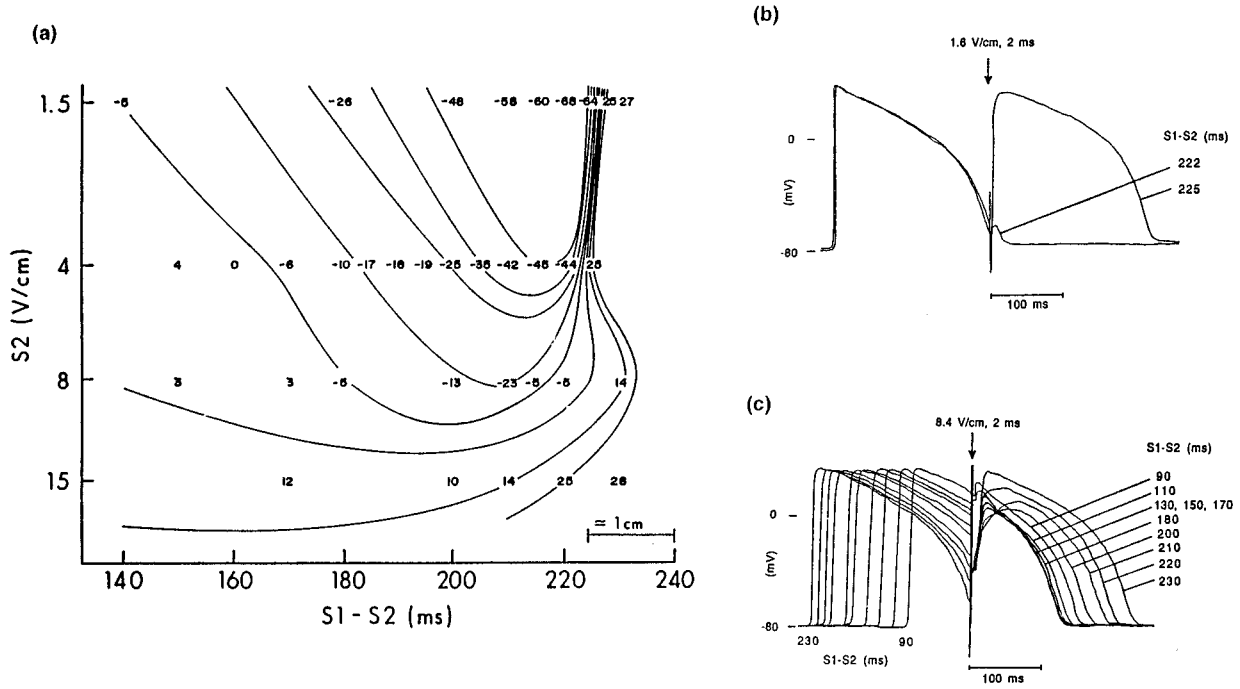

FIG. 14. (a) The map illustrating the changes of the transmembrane potential in a short strand caused by premature S2 shocks. Coupling intervals (S1-S2) are shown on a horizontal axis. The S2 strength is shown on a vertical axis (logarithmic scale). To be compatible with Fig. 5c, the weakest shocks are on the top and the strongest shocks are on the bottom. The isopotential contours, drawn in 10 mV increments, show the value of V_m 10 ms after the onset of S2, as measured by a microelectrode impaled in the center of the strand. (b) Action potential recordings illustrating the all-or-none type response to weak shocks. A 1.6 V/cm S2 shock was delivered at coupling intervals of 222 and 225 ms. The two recordings are aligned at the onset of S2. (c) Action potential recordings illustrating the response to strong shocks. Ten 8.4 V/cm shocks were delivered at coupling intervals of 90-230 ms. All recordings are aligned at the onset of S2. *Reproduced with permission from Knisley et al., Circ. Res.* ***70****, 707–715 (1992).*

B. Hypothesis—Heart as a collection of short fibers

The analysis conducted in the previous section gives a strong indication that the induction of rotors by cross-field stimulation cannot be attributed to a single mechanism. This section examines the hypothesis that the direct excitation of the distant tissue relies on the complex morphological structure of the heart and on the combined effect of several mechanisms.

This hypothesis is based on a similarity between the effects of premature shocks on a short, one-dimensional cardiac strand and on tissue exposed to the cross-field stimulation. Consider the experiment of Knisley *et al.*,[84] in which a guinea pig papillary muscle was used to study the changes in the action potential caused by S2 shocks delivered during the refractory period. By changing the S1-S2 interval and the strength of the S2 shock in a range comparable with Frazier's cross-field stimulation experiment,[4] Knisley *et al.* constructed the strength-interval map shown in Fig. 14a. In this map, the physiological state of the fiber is represented by the value of V_m 10 ms after the S2 shock. Weak shocks cause an all-or-none response (Fig. 14b) and, consequently, on the top of the map there is a sharp border between coupling intervals at which the shock excites the strand and intervals at which the shock leaves it unaffected. Strong shocks cause a graded response (Fig. 14c), so that on the bottom of the map, the coupling intervals at which S2 excites the strand lies next to the coupling intervals at which S2 prolongs refractoriness.

The comparison of Figs. 5c and 14a shows an intriguing correspondence between the dispersion of V_m measured in a short strand and the outcome of the cross-field stimulation performed on a whole heart. The position and the shape of the sharp border in Fig. 14a is the same as the position and the shape of the first post-shock wave front in Fig. 5c. In the lower part of Fig. 14a, strong shocks either excite the fiber or prolong its refractoriness and, correspondingly, there are no wave fronts initiated in the lower region of Fig. 5c. The responses typical for weak and strong shocks meet at approximately 5 V/cm, which is similar to the field strength of the critical point measured in Frazier *et al.*'s experiment. These qualitative and quantitative similarities may be a coincidence. However, they may also indicate that, in the cross-field stimulation experiments, the heart functions as a *collection* of short fibers.

According to such a hypothesis, groups of cells are organized into larger units, with a typical dimension of a few millimeters. Hence, the 3.4 by 3.4 cm region of Frazier *et al.*'s experiment would contain at least 10 by 10 units. There should be frequent electrical connections between cells within units and considerably less frequent connections between units. The spatial extent of these units should be on the order of a few length constants: small enough to allow electrotonic interactions and large enough for V_m induced by the shock to be relatively insensitive to the differences in their sizes. In such a structure, an electric shock would establish hyperpolarization and depolarization on the opposite ends of each unit, just like in a one-dimensional cable (Fig. 6b). Consequently, each unit would independently settle to a physiological state determined by the *local* electric field and

the *local* coupling interval. Since the field strength and the refractoriness change gradually, physiological states of the neighboring units would differ only slightly. However, there would be one exception: the units that were exposed to weak shocks during the critical phase of their action potential. Here, the S2 shock would directly excite the units that are closer to the S1 electrode and more recovered and leave unaffected units that are farther away and more refractory. The result would be a sharp border between units directly excited and unaffected by S2. Since these units are not totally isolated, this sharp border would give rise to a propagation of an action potential and a rotor would be initiated. Because the creation of a rotor involves many macroscopic units, the rotor would form on the length scale of centimeters, as observed in the experiments.

The support for the premise of our hypothesis, that the structural discontinuities can give rise to a physiologically significant transmembrane potential while still allowing the propagation of an action potential, comes from a recent study by Gillis *et al.*,[66] in which an optical mapping system was used to measure the response of the monolayers of ventricular myocytes to electric fields. The local lack of intercellular connections or the presence of a cleft gave rise to the shock-induced V_m, with hyperpolarized and depolarized regions in close proximity. However, these discontinuities did not prevent the propagation of an action potential, although a visible slowing was observed.

Is there any evidence that such macroscopic units might exist in a real heart? This hypothesis is supported by the complex morphological structure of the heart. First, the gross anatomy of the heart, coupled with an extensive network of veins and arteries, creates a structure in which major anatomical discontinuities occur every few millimeters. Second, histological evidence points out that cardiac fibers form ''unit bundles'' of diameters up to 200 μm that have no connections with the neighboring units bundles over distances of 200–560 μm.[85] Third, the collagen structure of the heart,[44,86,87] contributes to the separation of the myocardium into smaller units, separated by sheets of collagen running from endo- to epicardium. Fourth, the changing orientation of cardiac fibers and the fact that cardiac muscle has different anisotropy ratios in intra- and extracellular domains creates intertwined regions of hyperpolarization and depolarization. As evidenced by Fig. 5 of a paper by Trayanova *et al.* in this issue,[46] V_m in a two-dimensional slice of the heart exhibits a complicated spatial pattern in which depolarized and hyperpolarized regions exist within a few millimeters of each other, enabling interactions similar to those occurring in a short fiber. Finally, a similar ''patchy'' distribution of V_m has been shown to arise due to variation in the intracellular volume fraction.[88]

The experiments by Gillis *et al.*[66] who observed the regions of depolarization and hyperpolarization on the opposite sides of a cleft, and the experiments by White *et al.*[89] who demonstrated that the creation of a lesion decreases the local threshold for field stimulation, support our hypothesis of macroscopic inhomogeneities being an important factor in field stimulation. However, no one has yet performed a similar experiment on an intact heart. The polarization of the weakly coupled macroscopic units during a shock should be observable if mapped with millimeter spatial resolution. Zhou *et al.*[12] mapped V_m over the heart surface with a spatial resolution ranging from 30 μm to 3 mm. Yet, this study did not yield definite evidence, possibly because the measurements were made only at nine points on the epicardial surface. Until more detailed measurements of the shock-induced transmembrane potential are performed, evidence in support of the hypothesis that the heart acts as a collection of short fibers remains indirect.

VII. CONCLUSION

The mechanism of electrical stimulation is a central problem in cardiac electrophysiology. In this paper, the importance of this problem for the initiation of reentry in the heart was examined in the context of two case studies: reentry induced following unipolar stimulation and reentry triggered by cross-field stimulation. The first of these cases has a satisfactory explanation: a good agreement exists between the theoretical predictions of the bidomain model with unequal anisotropy ratios[37,43,75,90] and experimental observations of unipolar stimulation.[40–42,77] The initiation of reentry arises from a relatively straightforward combination of the bidomain model with the critical point theory.

The case of the reentry initiated by field stimulation does not yet have a satisfactory theoretical explanation. One reason is that the results of Frazier's study have not yet been fully confirmed by recordings with voltage-sensitive dyes. While several papers report the use of voltage-sensitive dyes in a cross-field stimulation setup, none of them gives a complete record of the activation sequence immediately after the shock. Most of these papers concentrate on such phenomena as the drift of rotors and thus present the evolution of rotors occurring later after the shock.[7,91] Knisley and Hill[8] report the activation sequence immediately following the shock. Unfortunately, the region of the heart mapped in this study is too small to confirm the existence and the extent of the region directly excited by the shock. A second reason is that the missing link, i.e., the mechanism by which electric shock can stimulate tissue away from the electrode, remains unknown. The effect of the sawtooth potential has been proposed as the mechanism for field stimulation, but the sawtooth has never been observed experimentally. Furthermore, there is evidence suggesting that the sawtooth mechanism alone is insufficient to explain the experimental observations related to the induction of rotors. Fiber curvature is another attractive candidate for the mechanism of field stimulation. However, theoretical studies of the transmembrane potential induced in a heart with a realistic fiber geometry have only just begun,[92] and experimental evidence for or against this mechanism does not yet exist. Macroscopic inhomogeneities may provide another mechanism for field stimulation; perhaps the most likely one. This mechanism is supported by recent experiments,[66,89] but has not yet been demonstrated to occur in an intact heart.

This review suggests that there is a critical lack of experimental evidence regarding the spatial distribution of a transmembrane potential during a shock. Both the sawtooth

potential at the cellular level and inhomogeneities at the macroscopic level provide telltale signatures that should be observable in a properly designed experiment. Ten years ago such experiments were not feasible because mapping studies could be performed only with extracellular recording electrodes.[4] Now, however, optical techniques are developed to a point where it should be feasible to map V_m with sufficient spatial resolution to determine the true mechanism of field stimulation.

ACKNOWLEDGMENTS

Supported in part by grants from the American Heart Association-Tennessee Affiliate and the Whitaker Foundation (B.J.R.) and by the NIH Grant No. HL54071, NSF Grant No. BES-940926, and NSF Engineering Research Center Grant No. CDR-8622201 (W.K.).

[1] A. T. Winfree, ''Sudden cardiac death: A problem in topology,'' Sci. Am. **248**, 144–161 (1983).
[2] A. T. Winfree, *When Time Breaks Down: The Three-Dimensional Dynamics of Electrochemical Waves and Cardiac Arrhythmias* (Princeton University Press, Princeton, 1987).
[3] A. T. Winfree, ''Electrical instability in cardiac muscle: Phase singularities and rotors,'' J. Theor. Biol. **138**, 353–405 (1989).
[4] D. W. Frazier, P. D. Wolf, J. M. Wharton, A. S. L. Tang, W. M. Smith, and R. E. Ideker, ''Stimulus-induced critical point: Mechanism for electrical initiation of reentry in normal canine myocardium,'' J. Clin. Invest. **83**, 1039–1052 (1989).
[5] N. Shibata, P-S. Chen, E. G. Dixon, P. D. Wolf, N. D. Danieley, W. M. Smith, and R. E. Ideker, ''Influence of shock strength and timing on induction of ventricular arrhythmias in dogs,'' Am. J. Physiol. **255**, H891–H901 (1988).
[6] P-S. Chen, P. D. Wolf, E. G. Dixon, N. D. Danieley, D. W. Frazier, W. M. Smith, and R. E. Ideker, ''Mechanism of ventricular vulnerability to single premature stimuli in open-chest dogs,'' Circ. Res. **62**, 1191–1209 (1988).
[7] J. M. Davidenko, P. F. Kent, D. R. Chialvo, D. C. Michaels, and J. Jalife, ''Sustained vortex-like waves in normal isolated ventricular muscle,'' Proc. Natl. Acad. Sci. USA **87**, 8785–8789 (1990).
[8] S. B. Knisley and B. C. Hill, ''Optical recordings of electrical stimulation on action potential repolarization and the induction of reeentry in two-dimensional perfused rabbit heart,'' Circulation **88**, 2402–2414 (1993).
[9] D. W. Frazier, W. Krassowska, P-S. Chen, P. D. Wolf, E. G. Dixon, W. M. Smith, and R. E. Ideker, ''Extracellular field required for excitation in three-dimensional anisotropic canine myocardium,'' Circ. Res. **63**, 147–164 (1988).
[10] J. P. Daubert, D. W. Frazier, P. D. Wolf, M. R. Franz, W. M. Smith, and R. E. Ideker, ''Response of relatively refractory canine myocardium to monophasic and biphasic shocks,'' Circulation **84**, 2522–2538 (1991).
[11] S. B. Knisley and B. C. Hill, ''Virtual electrode effects in myocardial fibers,'' Biophys. J. **66**, 719–728 (1994).
[12] X. Zhou, R. E. Ideker, T. F. Blitchington, W. M. Smith, and S. B. Knisley, ''Optical transmembrane potential measurements during defibrillation-strength shocks in perfused rabbit hearts,'' Circ. Res. **77**, 593–602 (1995).
[13] A. L. Hodgkin and W. A. H. Rushton, ''The electrical constants of a crustacean nerve fibre,'' Proc. R. Soc. B **133**, 444–479 (1946).
[14] S. Weidmann, ''Electrical constants of trabecular muscle from mammalian heart,'' J. Physiol. (London) **210**, 1041–1054 (1970).
[15] W. Krassowska, ''Modeling the interaction of cardiac muscle with strong fields,'' in *Case Studies in Mathematical Modeling–Ecology, Physiology and Biofluids*, edited by H. G. Othmer, F. R. Adler, M. A. Lewis, and J. C. Dallon (Prentice Hall, Upper Saddle River, NJ, 1997), pp. 277–308.
[16] C.-H. Luo and Y. Rudy, ''A model of the ventricular cardiac action potential: Depolarization, repolarization, and their interaction,'' Circ. Res. **68**, 1501–1526 (1991).
[17] P. G. Colavita, P. D. Wolf, W. M. Smith, F. R. Bartram, M. Hardage, and R. E. Ideker, ''Determination of effects of internal countershock by direct cardiac recordings during normal rhythm,'' Am. J. Physiol. **250**, H736–H740 (1986).
[18] D. P. Zipes, J. Fischer, R. M. King, A. Nicoll, and W. W. Jolly, ''Termination of ventricular fibrillation in dogs by depolarizing a critical amount of myocardium,'' Am. J. Cardiol. **36**, 37–44 (1975).
[19] T. Hoshi and K. Matsuda, ''Excitability cycle of cardiac muscle examined by intracellular stimulation,'' Jpn. J. Physiol. **12**, 433–446 (1962).
[20] E. Dekker, ''Direct current make and break thresholds for pacemaker electrodes on the canine ventricle,'' Circ. Res. **27**, 811–823 (1970).
[21] J. C. Schuder, H. Stoeckle, W. C. McDaniel, and M. Dbeis, ''Is the effectiveness of cardiac ventricular defibrillation dependent upon polarity?,'' Med. Instrum. **21**, 262–265 (1987).
[22] W. D. Weaver, J. S. Martin, M. J. Wirkus, S. Morud, S. Vincent, P. E. Litwin, and C. Morgan, ''Influence of external defibrillator electrode polarity on cardiac resuscitation,'' PACE **16**, 285–291 (1993).
[23] G. H. Bardy, T. D. Ivey, M. D. Allen, G. Johnson, and H. L. Greene, ''Evaluation of electrode polarity on defibrillation efficacy,'' Am. J. Cardiol. **63**, 433–437 (1989).
[24] S. A. Strickberger, J. D. Hummel, L. E. Horwood, J. Jentzer, E. Daoud, M. Niebauer, O. Bakr, K. C. Man, B. D. Williamson, and F. Morady, ''The effect of polarity on defibrillation threshold using a nonthoracotomy lead system,'' J. Am. Coll. Cardiol. **23**, 12A (1994).
[25] M. Usui, G. P. Walcott, S. A. Strickberger, D. L. Rollins, W. M. Smith, and R. E. Ideker, ''Effects of polarity for monophasic and biphasic shocks on defibrillation efficacy with an endocardial system,'' PACE, **19**, 65–71 (1996).
[26] P. G. O'Neill, K. A. Boahene, G. M. Lawrie, L. F. Harvill, and A. Pacifico, ''The automatic implantable cardioverter-defibrillator: effect of patch polarity on defibrillation threshold,'' J. Am. Coll. Cardiol. **17**, 707–711 (1991).
[27] R. K. Thakur, J. J. Souza, P. G. Chapman, P. J. Troup, and J. N. Wetherbee, ''Electrode polarity is an important determinant of defibrillation efficacy using a nonthoracotomy system,'' PACE **17**, 919–923 (1994).
[28] B. J. Roth, ''Mechanisms for electrical stimulation of excitable tissue,'' CRC Crit. Rev. Biomed. Eng. **22**, 253–305 (1994).
[29] E. A. Sobie, R. C. Susil, and L. Tung, ''A generalized activating function for predicting virtual electrodes in cardiac tissue,'' Biophys. J. **73**, 1410–1423 (1997).
[30] J. W. Woodbury and W. E. Crill, ''On the problem of impulse conduction in the atrium,'' in *Nervous Inhibition*, edited by L. Florey (Pergamon, Oxford, 1961), pp. 124–135.
[31] H. Shiba, ''An electric model for flat epithelial cells with low resistive junctional membranes. A mathematical supplement,'' Jpn. J. Appl. Phys. **9**, 1405–1409 (1970).
[32] L. Barr and E. Jakobsson, ''The spread of current in electrical syncytia,'' in *Physiology of Smooth Muscle*, edited by E. Bülbring and M. F. Shuba (Raven Press, New York, 1976), pp. 41-48.
[33] W. T. Miller, III and D. B. Geselowitz, ''Simulation studies of the electrocardiogram. I. The normal heart,'' Circ. Res. **43**, 301–315 (1978).
[34] L. Tung, ''A bi-domain model for describing ischemic myocardial D-C potentials'' Ph.D. dissertation, MIT, Cambridge, MA, 1978.
[35] B. J. Roth, ''Electrical conductivity values used with the bidomain model of cardiac tissue,'' IEEE Trans. Biomed. Eng. **44**, 326–328 (1997).
[36] B. J. Roth and J. P. Wikswo, Jr., ''The effect of externally applied electrical fields on myocardial tissue,'' Proc. IEEE **84**, 379–391 (1996).
[37] N. G. Sepulveda, B. J. Roth, and J. P. Wikswo, Jr., ''Current injection into a two-dimensional anisotropic bidomain,'' Biophys. J. **55**, 987–999 (1989).
[38] R. Plonsey and R. C. Barr, ''The four-electrode resistivity technique as applied to cardiac muscle,'' IEEE Trans. Biomed. Eng. **29**, 541–546 (1982).
[39] B. J. Roth, ''Approximate analytical solutions to the bidomain equations with unequal anisotropy ratios,'' Phys. Rev. E **55**, 1819–1826 (1997).
[40] M. Neunlist and L. Tung, ''Spatial distribution of cardiac transmembrane potentials around an extracellular electrode. Dependence on fiber orientation,'' Biophys. J. **68**, 2310–2322 (1995).
[41] S. B. Knisley, ''Transmembrane voltage changes during unipolar stimulation of rabbit ventricle,'' Circ. Res. **77**, 1229–1239 (1995).
[42] J. P. Wikswo, Jr., S-F. Lin, and R. A. Abbas, ''Virtual electrodes in cardiac tissue: A common mechanism for anodal and cathodal stimulation,'' Biophys. J. **69**, 2195–2210 (1995).
[43] B. J. Roth, ''Strength-interval curves for cardiac tissue predicted using the bidomain model,'' J. Cardiovasc. Electrophysiol. **7**, 722–737 (1996).
[44] P. J. Hunter, P. M. F. Nielsen, B. H. Smaill, and I. L. LeGrice, ''An anatomical heart model with applications to myocardial activation and ventricular mechanics,'' CRC Crit. Rev. Biomed. Eng. **20**, 403–426 (1992).

[45] N. A. Trayanova, B. J. Roth, and L. J. Malden, ''The response of a spherical heart to a uniform electric field: A bidomain analysis of cardiac stimulation,'' IEEE Trans. Biomed. Eng. **40**, 899–908 (1993).
[46] N. Trayanova, K. Scouibine, and F. Aguel, ''The role of cardiac tissue structure in defibrillation,'' Chaos **8**, 221–233 (1998).
[47] L. Clerc, ''Directional differences of impulse spread in trabecular muscle from mammalian heart,'' J. Physiol. (London) **255**, 335–346 (1976).
[48] L. Tung, N. Sliz, and M. R. Mulligan, ''Influence of electrical axis of stimulation on excitation of cardiac muscle cells,'' Circ. Res. **69**, 722–730 (1991).
[49] J. C. Neu and W. Krassowska, ''Homogenization of syncytial tissues,'' CRC Crit. Rev. Biomed. Eng. **21**, 137–199 (1993).
[50] J. M. Wharton, P. D. Wolf, W. M. Smith, P-S. Chen, D. W. Frazier, S. Yabe, N. Danieley, and R. E. Ideker, ''Cardiac potential and potential gradient fields generated by single, combined, and sequential shocks during ventricular defibrillation,'' Circulation **85**, 1510–1523 (1992).
[51] X. Zhou, J. P. Daubert, P. D. Wolf, W. M. Smith, and R. E. Ideker, ''Epicardial mapping of ventricular defibrillation with monophasic and biphasic shocks in dogs,'' Circ. Res. **72**, 145–160 (1993).
[52] E. Lepeschkin, H. C. Herrlich, S. Rush, J. L. Jones, and R. E. Jones, ''Cardiac potential gradients between defibrillation electrodes,'' Med. Instrum. **14**, 57 (1980).
[53] P-S. Chen, P. D. Wolf, F. J. Claydon III, E. G. Dixon, H. J. Vidaillet, Jr., N. D. Danieley, T. C. Pilkington, and R. E. Ideker, ''The potential gradient field created by epicardial defibrillation electrodes in dogs,'' Circulation **74**, 626–636 (1986).
[54] A. S. L. Tang, P. D. Wolf, Y. Afework, W. M. Smith, and R. E. Ideker, ''Three-dimensional potential gradient fields generated by intracardiac catheter and cutaneous patch electrodes,'' Circulation **85**, 1857–1864 (1992).
[55] R. Plonsey and R. C. Barr, ''Effect of microscopic and macroscopic discontinuities on the response of cardiac tissue to defibrillating (stimulating) currents,'' Med. Biol. Eng. Comp. **24**, 130–136 (1986).
[56] W. Krassowska, T. C. Pilkington, and R. E. Ideker, ''Periodic conductivity as a mechanism for cardiac stimulation and defibrillation,'' IEEE Trans. Biomed. Eng. **34**, 555–560 (1987).
[57] A. M. Chernysh, V. Y. Tabak, and M. S. Bogushevich, ''Mechanisms of electrical defibrillation of the heart,'' Resuscitation **16**, 169–178 (1988).
[58] S. M. Dillon, ''Optical recordings in the rabbit heart show that defibrillation strength shocks prolong the duration of depolarization and the refractory period,'' Circ. Res. **69**, 842–856 (1991).
[59] N. A. Trayanova and T. C. Pilkington, ''A bidomain model with periodic intracellular junctions: A one-dimensional analysis,'' IEEE Trans. Biomed. Eng. **40**, 424–433 (1993).
[60] J. P. Keener, ''Direct activation and defibrillation of cardiac tissue,'' J. Theor. Biol. **178**, 313–324 (1996).
[61] V. I. Krinsky and A. Pumir, ''Models of defibrillation of cardiac tissue,'' Chaos **8**, 188–203 (1998).
[62] Z. Lojewska, D. L. Farkas, B. Ehrenberg, and L. M. Loew, ''Analysis of the effect of medium and membrane conductance on the amplitude and kinetics of membrane potentials induced by externally applied electric fields,'' Biophys. J. **56**, 121–128 (1989).
[63] S. B. Knisley, T. F. Blitchington, B. C. Hill, A. O. Grant, W. M. Smith, T. C. Pilkington, and R. E. Ideker, ''Optical measurements of transmembrane potential changes during electric field stimulation of ventricular cells,'' Circ. Res. **72**, 255–270 (1993).
[64] H. Windish, H. Ahammer, P. Schaffer, W. Müller, and D. Platzer, ''Optical multisite monitoring of cell excitation phenomena in isolated cardiomyocyte,'' Pflugers Arch.-Eur. J. Physiol. **430**, 508–518 (1995).
[65] X. Zhou, W. M. Smith, D. L. Rollins, and R. E. Ideker, ''Spatial changes in transmembrane potential during a shock,'' PACE **18**, 935 (1995).
[66] A. M. Gillis, V. G. Fast, S. Rohr, and A. G. Kleber, ''Spatial changes in transmembrane potential during extracellular electrical shocks in cultured monolayers of neonatal rat ventricular myocytes,'' Circ. Res. **79**, 676–690 (1996).
[67] R. J. Matta, R. L. Verrier, and B. Lown, ''Repetitive extrasystole as an index of vulnerability to ventricular fibrillation,'' Am. J. Physiol. **230**, 1469–1473 (1976).
[68] J. P. Keener, ''On the formation of circulating patterns of excitation in anisotropic excitable media,'' J. Math. Biol. **26**, 41–56 (1988).
[69] M. S. Spach, W. T. Miller III, D. B. Geselowitz, R. C. Barr, J. M. Kootsey, and E. A. Johnson, ''The discontinuous nature of propagation in normal canine cardiac muscle. Evidence for recurrent discontinuities of intracellular resistance that affect the membrane currents,'' Circ. Res. **48**, 39–54 (1981).
[70] M. S. Spach and P. C. Dolber, ''The relation between discontinuous propagation in anisotropic cardiac muscle and the 'vulnerable period' of reentry,'' in *Cardiac Electrophysiology and Arrhythmias*, edited by D. P. Zipes and J. Jalife (Grune and Stratton, 1985), pp. 241–252.
[71] C. Cabo, A. M. Pertsov, J. M. Davidenko, and J. Jalife, ''Electrical turbulence as a result of the critical curvature for propagation in cardiac tissue,'' Chaos **8**, 116–126 (1998).
[72] A. Xu and M. R. Guevarra, ''Two forms of spiral-wave reentry in an ionic model of ischaemic ventricular myocardium,'' Chaos **8**, 157–174 (1998).
[73] A. T. Winfree, ''Ventricular reentry in three dimensions,'' in *Cardiac Electrophysiology, From Cell to Bedside*, edited by D. P. Zipes and J. Jalife (Saunders, Philadelphia, 1990), pp. 224–234.
[74] J. M. Saypol and B. J. Roth, ''A mechanism for anisotropic reentry in electrically active tissue,'' J. Cardiovasc. Electrophysiol. **3**, 558–566 (1992).
[75] B. J. Roth, ''Nonsustained reentry following successive stimulation of cardiac tissue through a unipolar electrode,'' J. Cardiovasc. Electrophysiol. **8**, 768–778 (1997).
[76] G. W. Beeler and H. Reuter, ''Reconstruction of the action potential of ventricular myocardial fibres,'' J. Physiol. (London) **268**, 177–210 (1977).
[77] S-F. Lin, B. J. Roth, D. S. Echt, and J. P. Wikswo, Jr., ''Complex dynamics following unipolar stimulation during the vulnerable phase,'' Circulation **94**, I–714 (1996).
[78] L. V. Chernomordik and Y. A. Chizmadzhev, ''Electrical breakdown of lipid bilayer membranes. Phenomenology and mechanism,'' in *Electroporation and Electrofusion in Cell Biology*, edited by E. Neumann, A. E. Sowers, and C. A. Jordan (Plenum Press, New York, 1989), pp. 83–95.
[79] O. Tovar and L. Tung, ''Electroporation of cardiac cell membranes with monophasic or biphasic rectangular pulses,'' PACE **14**, 1887–1892 (1991).
[80] S. B. Knisley, ''Transmembrane potentials at the ends of ventricular myocytes during electroporation by field stimulation,'' PACE **17**, 838 (1994).
[81] W. Krassowska, ''Effects of electroporation on transmembrane potential induced by defibrillation shocks,'' PACE **18**, 1644–1660 (1995).
[82] W. Krassowska and M. S. Kumar, ''The role of spatial interactions in creating the dispersion of transmembrane potential by premature electric shocks,'' Ann. Biomed. Eng. **25**, 949–963 (1997).
[83] M. G. Fishler, E. A. Sobie, L. Tung, and N. V. Thakor, ''Modeling the interaction between propagating cardiac waves and monophasic and biphasic field stimuli: The importance of the induced spatial excitatory response,'' J. Cardiovasc. Electrophysiol. **7**, 1183–1196 (1996).
[84] S. B. Knisley, W. M. Smith, and R. E. Ideker, ''Effect of field stimulation on cellular repolarization in rabbit myocardium: Implications for reentry induction,'' Circ. Res. **70**, 707–715 (1992).
[85] J. R. Sommer and B. Scherer, ''Geometry of cell and bundle appositions in cardiac muscle: light microscopy,'' Am. J. Physiol. **248**, H792–H803 (1985).
[86] P. C. Dolber and M. S. Spach, ''Conventional and confocal fluorescence microscopy of colagen fibers in the heart,'' J. Histochem. Cytochem. **41**, 465–469 (1993).
[87] I. J. LeGrice, B. H. Smaill, L. Z. Chai, S. G. Edgar, J. B. Gavin, and P. J. Hunter, ''Laminar structure of the heart: ventricular myocyte arrangement and connective tissue architecture in the dog,'' Am. J. Physiol. **269**, H571–H582 (1995).
[88] M. G. Fishler, ''Membrane polarization induced by heterogeneity of tissue anisotropy: Model reveals an additional mechanism underlying 'far-field' stimulation during defibrillation-level shocks,'' PACE **20**, 1195 (1997).
[89] J. B. White, G. P. Walcott, and R. E. Ideker, ''Myocardial discontinuities: A substrate for producing virtual electrodes to increase directly excited areas of the myocardium by shocks,'' PACE **20**, 1234 (1997).
[90] B. J. Roth, ''A Mathematical model of make and break electrical stimulation of cardiac tissue by a unipolar anode or cathode,'' IEEE Trans. Biomed. Eng. **42**, 1174–1184 (1995).
[91] A. M. Pertsov, J. M. Davidenko, R. Salomonsz, W. T. Baxter, and J. Jalife, ''Spiral waves of excitation underlie reentrant activity in isolated cardiac muscle,'' Circ. Res. **72**, 631–650 (1993).
[92] N. Trayanova, J. Eason, and C. S. Henriquez, ''Electrode polarity effects on the shock-induced transmembrane potential distribution in the canine heart,'' in *Proceedings of the 17th Annual Conference of the IEEE Engineering in Medicine and Biology Society* (IEEE, Piscataway, NJ, 1995), pp. 317–318.